forschen.
vernetzen.
anwenden.

Innovationsreport 2024

Industrielle Gemeinschaftsforschung

IGF-Forschungsvorhaben 324 EN

CORNET: Entwicklung von neuen antibakteriell funktionalisierten Textilien und 3D-gedruckten Filtern für die Prozesswasseraufbereitung

Development of new antibacterial functionalised textiles and 3-D-printed filters for process water treatment (DAF3D)

Laufzeit:

01.01.2022 – 31.12.2023

Beteiligte Forschungsstelle(n):

Institut für Umwelt & Energie, Technik & Analytik e.V. (IUTA)
Forschungsabteilung Forschungsanalytik & Miniaturisierung

(sowie belgische Partner)

iuta.de

Schlussbericht vom 27.05.2024

zu IGF-/ CORNET-Vorhaben Nr. 324 EN

Thema

Entwicklung von neuen antibakteriell funktionalisierten Textilien und 3D-gedruckten Filtern für die ProzesswasseraufbereitungEntwicklung von neuen antibakteriell funktionalisierten Textilien und 3D-gedruckten Filtern für die Prozesswasseraufbereitung

Development of new antibacterial functionalised textiles and 3-D-printed filters for process water treatment (DAF3D)

Berichtszeitraum

01.01.2022 - 31.12.2023

Forschungsvereinigung

Institut für Umwelt & Energie, Technik & Analytik e. V

Forschungseinrichtung(en)

FE 1: Institut für Umwelt & Energie, Technik & Analytik e. V

Sowie internationale Partner aus Belgien:

CELABOR,

University of Liège, NCE

Gefördert durch:

Bundesministerium für Wirtschaft und Klimaschutz

aufgrund eines Beschlusses des Deutschen Bundestages

Table of contents

Figures

Tables

List of abbreviations

Abbreviation	Meaning
ASA	Acrylonitrile styrene acrylate
AZO	Aluminium-doped ZnO
BOD5	Biochemical oxygen demand
DBP	Disinfection by-products
DWA	Deutsche Vereinigung für Wasserwirtschaft, Abwasser und Abfall e. V. (German Association for Water, Wastewater and Waste)
E. coli	Escherichia coli
EU WFD	European Water Framework Directive
FDA	US Food and Drug Administration
FWMH	Full width at half maximum
HMTA	Hexamethylenetetramine
NBT	Nitro blue tetrazolium
NP	Nanoparticle
PA	Polyamide
PL	Photoluminescence
PLA	Polylactic acid
PLE	Photoluminescence excitation
PMMA	Poly(methyl methacrylate)
PNP	Para-nitrophenol
SEM	Scanning electron microscopy
SME	Small and medium-sized enterprises
TRD	Technische Regeln für Dampfkessel (Technical Regulations for steam boilers)
UV	Ultraviolet
VDI	Verein Deutscher Ingenieure e.V. (The Association of German Engineers)
VdTÜV	Technischer Überwachungsverein-Verband (Association of Technical Inspection Agencies)
WP	Work Package
ZnO	Zinc Oxide

1. Presentation of the research program and objectives

Water is vital for life and the essential key to important industrial processes. Due to the increasing consumption and contamination, water access, treatment, and safety is becoming challenging and costly. Therefore, new technologies must be developed to ensure sustainable protection and safe access to water for both human consumption and industrial use (European Commission, 2012; 2022). The DAF3D project aims to develop an innovative and sustainable 3D-printed filter based on antibacterial functionalised textiles for water disinfection. The expected application is centred on production and reuse of process water from diverse industrial sectors and grey water within households. In chemical and food industries, for example, water recycling is enforced and reduces costs simultaneously, but biological safety is a major concern. Thus, the 3D-printed filter composed of antibacterial functionalised textiles is a promising solution for these issues and can be implemented in a wide array of applications, configurations, and dimensions.

The innovative disinfection filter consists of a thermoplastic for 3D-printing in combination with textile materials pre-impregnated with antibacterial agents as zinc oxide (ZnO) structures. These new antibacterial textiles are capable of generating highly reactive oxidizing species in situ, that degrade a wide range of organic substances, including microorganisms (Gudkov et al, 2021). It has been shown that ZnO can be used for water hygienisation due to its antimicrobial capacity. Species generated by ZnO migrate through the cell wall, causing irreversible damage and leading to cell death.

Additive manufacturing technologies are capable of printing filter materials with precisely defined structures. The innovative principle behind this manufacturing process allows for development of efficient flow paths through the filter and the possible incorporation of additives for expanding and enhancing functionality and reactivity. However, several aspects must be considered when applying such materials to water disinfection, as the risk of degradation and leaching would cause severe problems. Therefore, this project aims to develop innovative materials that can be used for water hygienisation without causing contamination. A material with these properties is not yet available on the market. Therefore, antibacterial textile micropowders based on ZnO will be incorporated into the thermoplastic compound at different concentrations using a plastic extruder. Subsequently, a filament for 3D-printing will be produced to support further manufacturing of the filter for process water disinfection.

The developed antibacterial filter will be tested for the degradation of microorganisms, such as E. *coli* and other pathogens individually and/or in combination, in a variety of domestic and industrial process waters. Pretreatments will be applied before the filter, depending on the process water to be treated. The tests will be performed in a bench scale demonstrator. The

treated water will be accessed accordingly to evaluate disinfection efficiency and the reusability in the targeted industrial sector.

In summary, the ultimate aim of the DAF3D project is to develop and evaluate a disinfection filter for process water reuse. This will be achieved by combining functionalised textiles impregnated with antimicrobial agents and a suitable thermoplastic for 3D-printed filters. The versatility of 3D-printed antimicrobial filter will support SMEs in market creation. In addition, the filter is a promising and competitive technology to replace less efficient and sustainable existing technologies. Furthermore, the flexibility will enable and/or increase the application of water recycling and reuse in industrial and private applications. The DAF3D project can have a significant impact on enabling sustainable treatment and safe access to water, an essential resource that is vulnerable to contamination and source of critical health and environmental problems.

The project is divided into 8 work packages (WP). The structure of the project and the sequence of work packages is shown in Figure 1.

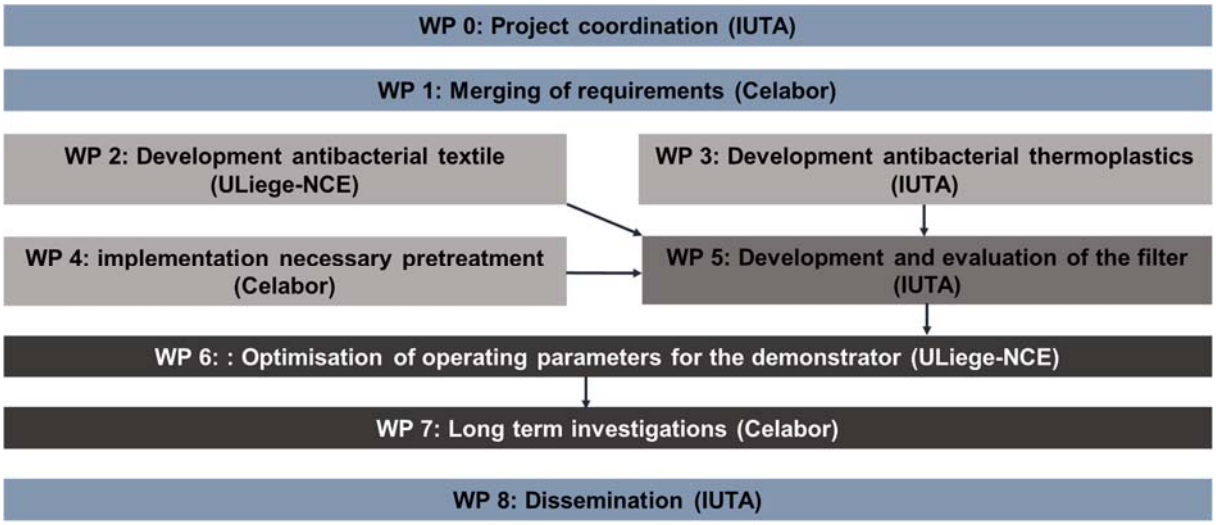

Figure 1: Overview of the DAF3D work packages.

The partners of the project are:

- Institut für Umwelt & Energie, Technik & Analytik e. V. (IUTA), North Rhine-Westphalia, Germany) - Coordinator
- CELABOR (Herve, Wallonia, Belgium)
- ULG-NCE (University of Liege, Department of Chemical Engineering – Catalysis, Nanomaterials, Electrochemistry, Liege, Wallonia, Belgium)

2. State of the art and technological alternatives

Currently available methods for process water disinfection do not meet all the requirements to further promote water recycling and reuse in the industry. For example, chemical treatments, such as chlorination, are widely used and efficient, but the formation of toxic and often unknown disinfection by-products (DBP) is a major concern. Ozonation can also be used for water disinfection. One of the most applied techniques is UV treatment, which inactivates biohazards, leading to the reduction of cultivable/reproducible bacteria. The main disadvantage of the UV disinfection is the high cost of operation. Membrane technologies have emerged as the favoured choice for reclaiming water from different wastewater streams. These treatments have drawbacks such as membrane cleaning and fouling as well as a high energy demand. Particularly for smaller volumes of water, the cost increases significantly.

In 2014, Wang et al. published a review of materials that can be used for textile applications. ZnO appeared as a potential antimicrobial agent. Moreover, in a more recent article (2019), Verbic et al. summarized the outstanding properties of ZnO. These comprise a remarkable thermal and UV stability, its biocompatibility, environmental friendliness, the acceptance by the Food and Drug Administration (FDA) and its low cost. These properties make it a candidate of choice for the synthesis of antibacterial, self-cleaning, depolluting or anti-UV composites. The antimicrobial mechanism of ZnO is complex. While the generation of highly reactive oxygen species plays an essential role in the antimicrobial activity, it is known that the dissolution of ZnO molecules and subsequent release of Zn^{2+} ions can inhibit the respiratory mechanism of bacteria and it has been shown that ZnO nanoparticles, once adsorbed on the wall of a bacterium, can disrupt it without the aid of light activation. Verbic et al. conclude their review by stating that ZnO is one of the most promising materials for the development of high-performance antibacterial textiles. Doping of ZnO with transition metals such as Mn, Cu, Co, Fe and Al results in promising antibacterial properties.

Kezhen Qi et al. (2020) showed a reduction of log 7 for E. *coli* in 24 h with a load of 500 mg/L Cu-ZnO. The antimicrobial effect is due to the accumulation of Cu-ZnO particles on the surface of the membrane, which prevents bacterial growth. The Cu-ZnO particles attract the bacterial membranes of E. *coli* by electrostatic interactions because Cu-ZnO particles have a positive charge, and the bacterial membranes have a negative charge. Furthermore, the use of structured coatings of aluminium-doped ZnO (AZO) on PLA fibres (Valerini et al., 2020) have shown very interesting antibacterial properties. In the AZO material, aluminium atoms can replace zinc atoms in the ZnO lattice (forming $ZnAl_2O_4$) or induce the formation of alumina (Al_2O_3), which could contribute to enhance antimicrobial properties through increased water vapor barrier properties.

Within the framework of the cornet project BACZEREAU, ULiege-NCE develops different formulations based on ZnO and doped with Fe^{3+} and Cu^{2+} ions. These formulations are coated on INOX 316L supports by spray-coating. These coatings are used for the disinfection of natural bathing waters with the use of visible light. At this stage, from the first results obtained on coatings of $ZnFe_2O_4$, a two-log reduction is observed for bacteria population after 2 h at 15 °C at a wavelength equal to 395 nm. Concluding, the first results obtained in BACZEREAU were the basis to select the best structure of ZnO (e.g. spheres and wires). The aim is to obtain a high specific surface area for its application as an antimicrobial agent in the DAF3D project for process water disinfection.

Additive manufacturing will be used in this project to tailor filters with a structured morphology. A benefit of 3D-printing is the ability to achieve complex geometries. Low production volumes can be manufactured cost-effectively, reducing investment in tooling, for example. The flexibility and speed of 3D-printing allows a rapid iteration of geometries and parts to be produced quickly. (Kristiawan et al, 2021)

The additive manufacturing technique that is applicable to this project is material extrusion. Material extrusion is a form of 3D-printing that utilizes filaments, a type of thermoplastic, to create complex structures. In this process material is dispensed through a nozzle onto a build platform where the material solidifies. The nozzle then moves, in combination with the build platform, while dispensing material to build up the desired form. If required, it is possible to print a part with dissolvable support material. This requires the implementation of two toolheads to avoid cross-contamination of the materials. Depending on the support material, it can be removed mechanically, or it can be dissolved in either water or an organic solvent.

An important aspect of material extrusion is layer bonding. Layers need to bond and solidify with the previously printed material. The downward force from the nozzle and the partial re-melting of the underlying material allows the new layer to bond with the previously printed layer. A drawback to material extrusion is that the produced parts have anisotropic material properties, since parts are built up in layers.

The quality of the surface finish, produced by this technique, must be considered while deciding how to produce a part. When a smooth surface finish is desired then a small layer height should be selected. Common layer heights for material extrusion and vat photopolymerization are within 0.05 mm – 0.4 mm and 0.025 mm – 0.1 mm, respectively. The decrease in layer height is also accompanied with an increase in cost and print time.

Since the beginning of this project several new materials for additive manufacturing appeared on the market. Most of these materials are still based on PLA, which is not suitable regarding the requirements of this project. PLA starts to deform at a temperature of 60 °C and water has a long-term degrading effect on the material. Additionally, a chlorinated polyethylene (CPE) (Fiberlogy, Poland), and a thermoplastic polyurethane (TPU) (Copper3D, Chile) have entered the market. Both are closer to thermoplastic elastomers than engineering plastics, of which there is currently no antibacterial variant on the market.

3. Detailed presentation of the results achieved by the funding, taking the defined objectives into account

In chapter 3 the results of each work package are given.

3.1 WP 1: Merging of national and European requirements for process water reuse (Celabor)

During WP 1 relevant industrial sectors with the corresponding requirements should be determined. In addition, the information from the research should be presented in a detailed table.

3.1.1 Task 1.1: Research of requirements for industrial sectors

Water resources and supplies in the EU are coming under increasing pressure due to climate change, leading to water scarcity and droughts. Across the EU, water scarcity and droughts are expected to become more frequent and severe in the future. Around the Mediterranean, more than 50 % of the regions are affected by water stress. Water is increasingly being reused in industry, directly or after treatment, for its own reuse within a company or between companies.

The main legislation on water reuse in Belgium and Germany is the European Water Framework Directive 2000 (EU WFD), Regulation EU 2020/741 on minimum requirements for water reuse and the European Green Deal.

The EU WFD lists sectors where the implementation of water reuse measures can be beneficial. These include:

- Agriculture,
- Urban environment (recreation and irrigation, firefighting) and
- Industry (washing of machinery and equipment).

However, quality requirements for water reuse are not specified. Rather, good chemical and ecological status of water bodies is the main objective. Minimum requirements for water reuse have been set in Regulation EU 2020/741. The aim of this regulation is to:

- ensure that reused water is safe for agriculture, animals, and humans,
- facilitate water reuse where it is appropriate, environmentally friendly, and cost-effective; and
- recover nutrients from reused water and apply them to crops, thereby reducing the need for mineral fertilisers.

Specific quality requirements for water reused for irrigation are defined for E. *coli*, legionella, BOD5 and suspended solids. Water reuse can be a valuable measure to combat water scarcity. Regulation EU 2020/741 has been implemented since 26 June 2023. However, the

regulation does not apply to industrial water reuse. The European Green Deal calls for circular approaches to water reuse in agriculture and industrial processes. This includes an integrated nutrient management plan to ensure a more sustainable use of nutrients and to stimulate markets for recovered nutrients.

In Belgium, there are no further national or sector-specific regulations. In Germany, on the other hand, there are some industrial sectors where the reuse of industrial water is regulated separately by EU regulations. In most cases, industrial water must comply with the Drinking Water Ordinance. Food production, for example, requires desalination and the reduction of organic impurities. In the food and brewing industries, even if the process water is used only for cleaning purposes, the reused process water must be of drinking water quality.

The different regulations were summarised in a comparative table with European and national regulations and discussed with the members of the project monitoring committee. This will enable the SMEs and the project partners to set treatment targets and to assess the quality achieved on a sector-specific basis in the course of further investigations.

In addition, potential industrial sectors for the use of the filters were identified within the framework of WP 1 and the following practical partners were recruited:

- Reuse of cleaning water: Car wash (Hydroliege), textile cleaning (Depairon and Waretex GmbH), tank cleaning (ASRO-CLEAN);
- Beverage industry: breweries (Lefebvre Brewery, Webster Brewery);
- Food industry (Walhorn);
- Paper industry: Essity and Alhstrom.

3.1.2 Task 1.2: Creation of a comprehensive table

Some laws, standards and regulations on water quality requirements are summarised in the following Table 1.

Table 1: Summary of national and international standards for the reuse of industrial water.

Guide	Year	Application area
Code of practice DWA-M 1200	Since 9th September of 2020 in preparation	Part 1: Principles of water reuse for different users (KA-8). Part 2: Requirements for advanced wastewater treatment (KA-8). Part 3: Utilization of clear water for irrigation in agriculture, horticulture and green areas (GB-5).
National Water Strategy (Nationale Wasserstrategie)	2021	Application of EU Legislation (EU VO 2020/741). The development of guidelines for water reuse and multiple uses (e.g., precipitation water) in municipal land use planning and water supply concepts for urban districts is envisioned.
Bundesgesetzblatt zu Brauchwasser	15.02.1975	Requirements for process water are the same ones for drinking water
EU Regulation in progress	2020	Regulation for water reuse out of waste water and surface water bodies for agriculture
Marktpotenziale der Wasserwiederverwendung	2017	Target market study for water reuse in MULTI-ReUse process
Richtlinienreihe VDI 3803 "Raumlufttechnik, Geräteanforderungen"	2020	Process water in ventilation
Richtlinienreihe VDI 2047 "Hygiene bei Rückkühlwerken"	2021	Process water hygiene in cooling towers
DIN EN 12953-10 Großwasserraumkessel: Anforderungen an die Speisewasser- und Kesselwasserqualität	2003	Standard for process water in shell boilers
DIN EN 12952-12 Wasserrohrkessel: Anforderungen an die Speisewasser- und Kesselwasserqualität	2003	Standard for process water in water tube boilers
TRD 611 Speisewasser und Kesselwasser von Dampferzeugern	1996	Standard for process water in boilers
VdTÜV MB TECH 1453 VdTÜV-Richtlinien für Speisewasser, Kesselwasser und Dampf von Dampferzeugern bis 68 bar zulässigem Betriebsüberdruck	1983	Standard for process in steam reactors
VGB R 450 L Speisewasser-, Kesselwasser- und Dampfqualität für Kraftwerke/Industriekraftwerke	2023	Standard for process water in power plants
Trinkwasserverordnung Anlage 1 und 2	2021	Limit values for bacteria concentration: E.Coli 0/250 mL; Entercoccus 0/250 mL; Pseudomonas aeruginosa 0/250 mL
Urban wastewater treatment (COM (2022) 541 final)	2024	Reduction of 12 selected micropollutants by 80% -> upgrade for WWTP > 100,000 PE

3.2 WP 2: Development of antibacterial textiles (ULiege-NCE)

Work package 2 focuses on the production of pure and doped ZnO structures. In addition, antibacterial textiles are to be developed.

3.2.1 Task 2.1: Synthesis and characterization of ZnO structures

The first type of synthesis tested is further referred to as Pepti or ZnO-A.

5.9 g of zinc acetate dihydrate ($Zn(CH_3COO)_2.2H_2O$, VWR CHEMICALS, Netherlands) is dissolved in 250 mL at 80 °C, with stirring. At the same time, 4.5 g of KOH is dissolved in 130 mL of ethanol. After dissolving each compound, KOH is added dropwise to the zinc acetate solution and allowed to react for 2 h. The solution is then washed three times with ethanol and oven-dried for 12 h at 100 °C to obtain a powder.

The second synthesis method is called Polyol or ZnO-B.

Zinc acetate dihydrate is dissolved in diethylene glycol ($C_4H_{10}O_3$, MERCK, Germany), to reach a concentration of 30 g/L of zinc oxide. Starting from room temperature, it is raised up to 140 °C to achieve complete dissolution. After the temperature reaches 180 °C and the solution becomes opaque and white, the reaction takes place for 2 h while keeping the temperature at that level. The suspension is then washed three times with ethanol and the resulting powder is dried at 100 °C for 12 h.

The third method is called Orga or ZnO-C.

Zinc acetate dihydrate is dissolved in ethanol by adding ethanolamine (EA) at room temperature. In a typical synthesis, 10.976 g of ZnAc and 3.05 g of EA are mixed in 160 g of ethanol. The precursor solution is heated at 60 °C for 2 h. Since the zinc oxide is not formed directly in the solution, a thermal treatment is required in order to form it, which is done at 550 °C for 2 h resulting in a white powder.

Nanorods and Nanodisks can also be separated by synthesis.

As described in the literature, Hexamethylenetetramine (HMTA) acts as a source of hydroxide. Under the effect of temperature, HMTA decomposes into formaldehyde and ammonia. The latter reacts with water in order to form hydroxide ions which could react with Zn^{2+} ions to form zinc hydroxide. The following equations summarise this mechanism:

$$C_6H_{12}N_4 + H_2O \rightarrow 6\ CH_2O + 4\ NH_3$$

$$NH_3 + H_2O \rightarrow NH_4OH$$

$$2\ OH^- + Zn^{2+} \rightarrow Zn(OH)_2$$

Zinc oxide is directly formed by the zinc hydroxide, which is the site of the crystallisation of the catalytic material.

Different morphologies can be obtained by varying only the concentration of the precursors, since the temperature and time of the two reactions remain constant. For the nanorods, 3 g of zinc acetate and 1.92 g of HMTA are dissolved in 360 mL of deionised water. The solution is heated at 90 °C for 12 h. The same procedure is used to synthesize nanodisks, but 24 mL of water is used instead of 360 mL.

A Flower-Like form can also be synthesized.

Zinc nitrate (3 g) is dissolved in water (100 mL) while stirring. When the zinc nitrate is completely dissolved, NaOH 1.5 M is quickly added to the solution. The reaction takes place for 2 h at room temperature. The resulting powder is washed several times with ethanol and dried in an oven.

After synthesis the materials are further treated since oxygen vacancies are of great importance for the antibacterial efficiency of the catalyst in the dark. For this purpose, the powder synthesised in the ZnO-A synthesis is used. The treatment consists of adding $NaBH_4$, a reducing agent, to the ZnO powder in different molar ratios. $NaBH_4$ reacts with the zinc to reduce it, increasing the amount of oxygen vacancies.

The materials are characterized by different methods, starting with X-Ray Diffraction.

Crystallite structure and phases are determined using Bruker D8 Twin-Twin X-Ray Diffractometer with a (Cu-K_α) radiation of 1.54 Å in a range between 2Θ = 10 to 70 °. The crystallite size of the different samples is estimated using the Scherrer formula. The percentage of crystallinity of the different powders is estimated using the Rietveld refinement method.

XRD patterns, presented in Figure 2, show the characteristic peaks of the zinc oxide in the wurtzite structure for the three samples with the three main peaks located between 2Θ = 30 ° to 40 °. The diffractogram corresponding to ZnO-A, shows peaks with a larger full width at half maximum height (FWMH) than the other two catalysts, indicating a smaller crystallite size. The sizes are 5 nm for ZnO-A compared to 18 nm for ZnO-B and 60 nm for ZnO-C.

The three main peaks show different intensities between the samples. The higher intensity of the peaks for the ZnO-C can be explained by the thermal treatment at 550 °C which increases the crystallite size of the powder. Figure 3 shows nanorods (NR), nanodisks (ND) and Flower-Like zinc oxide (FL).

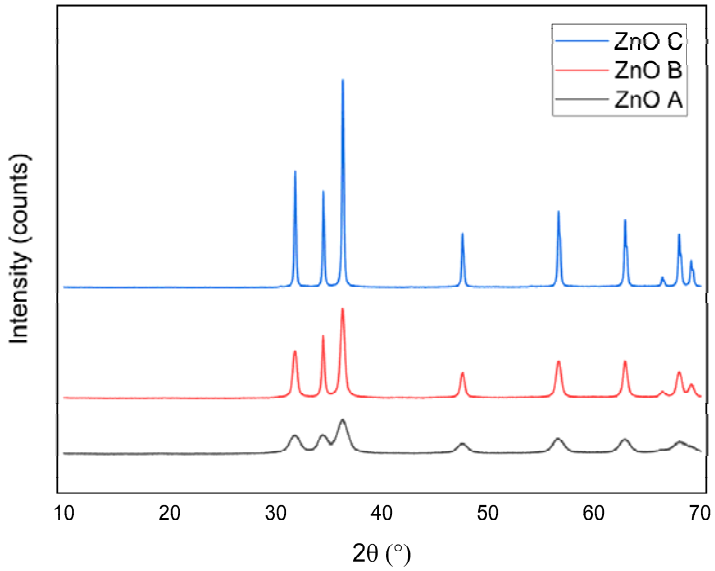

Figure 2: Diffractograms of ZnO-A (Pepti), ZnO-B (Polyol) and ZnO-C (Orga).

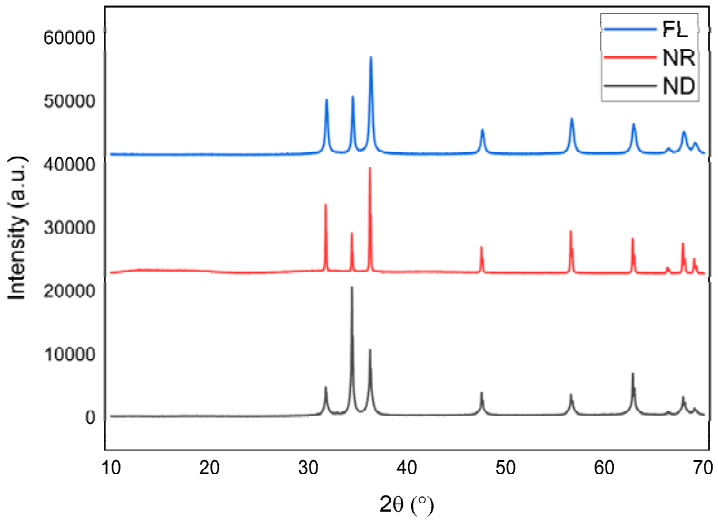

Figure 3: Diffractograms for ZnO Nanodisks (ND), Nanorods (NR) and Flower-Like structures (FL).

There is a significant difference in the diffractograms of NR and ND. The zinc oxide is present in its wurtzite form with the same characteristic peaks as before. However, there is a noticeable difference in intensity between the peaks located at 2Θ from 30 ° to 40 ° in NR and ND. This is due to the different preferred growth directions in different planes. This is illustrated in the following Figure 4:

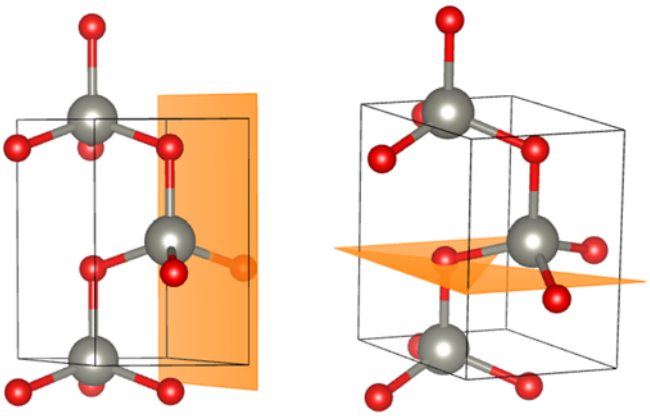

Figure 4: Preferential growth plan for NR (left), and the preferential growth plan for ND (right).

The morphologies of the three powders were also analysed by Scanning Electron Microscopy (SEM) (Bruker TESCAN CLARA, Czech Republic). The samples are dispersed in acetone by ultrasonic waves for 2 min, and then placed on a glass slide divided into eight parts. The latter is sputtered with gold before being placed in the microscope. The images are shown in Figure 5.

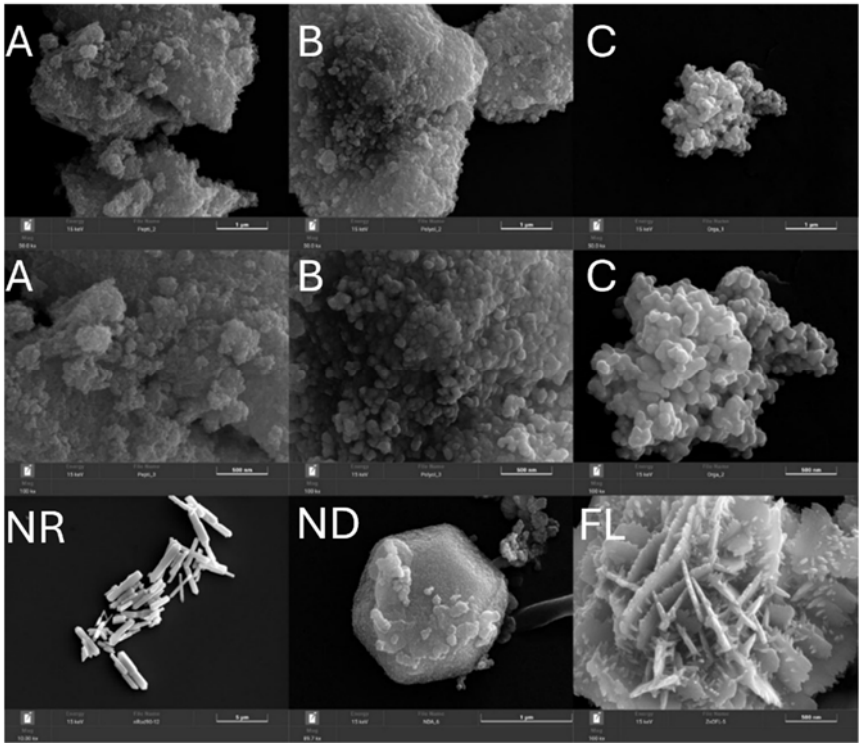

Figure 5: SEM images corresponding to ZnO samples A, B and C, NR, ND and FL. The top images correspond to a magnification of 50 kx, the middle images to 100 kx of ZnO-A, B and C. The scales are shown on the different pictures. The three SEM images in the lowest row have varying magnification to highlight the shape of the particles instead of the size differences.

The ZnO-A, B and C show spherical morphology with small particle aggregates forming larger ones. A particle of the ZnO-A is smaller than the particles from samples B and C. This is consistent with the size of the crystallites of these three samples. The difference in reagent concentration leads to different morphologies, as can be seen in the NR and ND images.

Nitrogen adsorption-desorption isotherms were collected on a micromeritics ASAP 2420 at a temperature of 196 °C, as seen in Figure 6 and Table 2. Before, samples were degassed under high vacuum at 80 °C for 15 h. The specific surface area, S_{BET}, was determined using the Brunauer Emmett and Teller (BET) equation by taking the relative pressure data between 0.05 and 0.25.

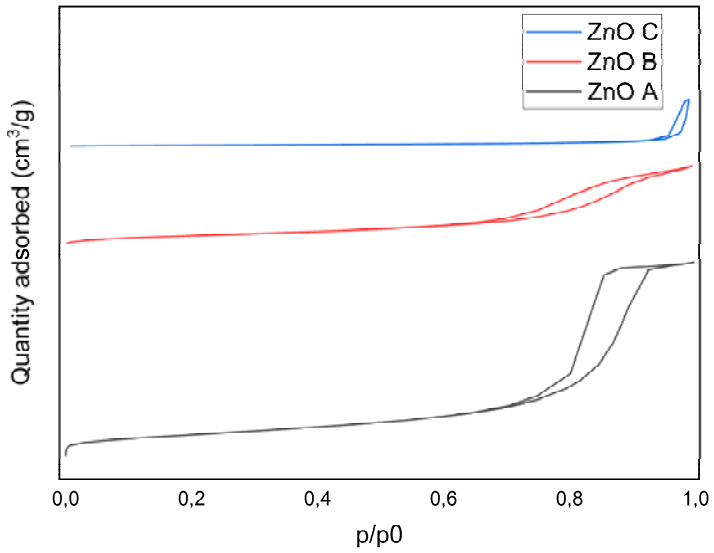

Figure 6: Sorption isotherms for ZnO-A, B and C samples. For further details.

The nitrogen adsorption/desorption isotherms allow the measurement of the specific surface area values via the BET equation:

Table 2: Listing of the different specific surface areas of the samples as well as the crystallite size and percentage of crystallinity.

Samples	S_{BET} (m^2/g)	d_{cryst} (nm)	%cryst
Polyol	40	15	70
Pepti	90	5	83
Orga	6	60	68
FL	8	28	-
NR	0.8	-	-

Photoluminescence emission (PL) and excitation (PLE) spectra were measured using an Edinburgh FS920 fluorescence spectrometer (Edinburgh Instruments Ltd, Livingston, UK), and a 450 W xenon arc lamp as excitation source. Samples were fixed to a metal plate using a double-sided tape. The wavelength of the incident light is the same for the three samples to be analysed, i.e. 325 nm. Measurements were made over a range of 350 nm to 800 nm in 0.5 nm steps, allowing the entire zinc oxide gap to be scanned. The experiments were performed at room temperature. In the following Figure 7 the obtained spectra were analysed using OriginPro Lab software.

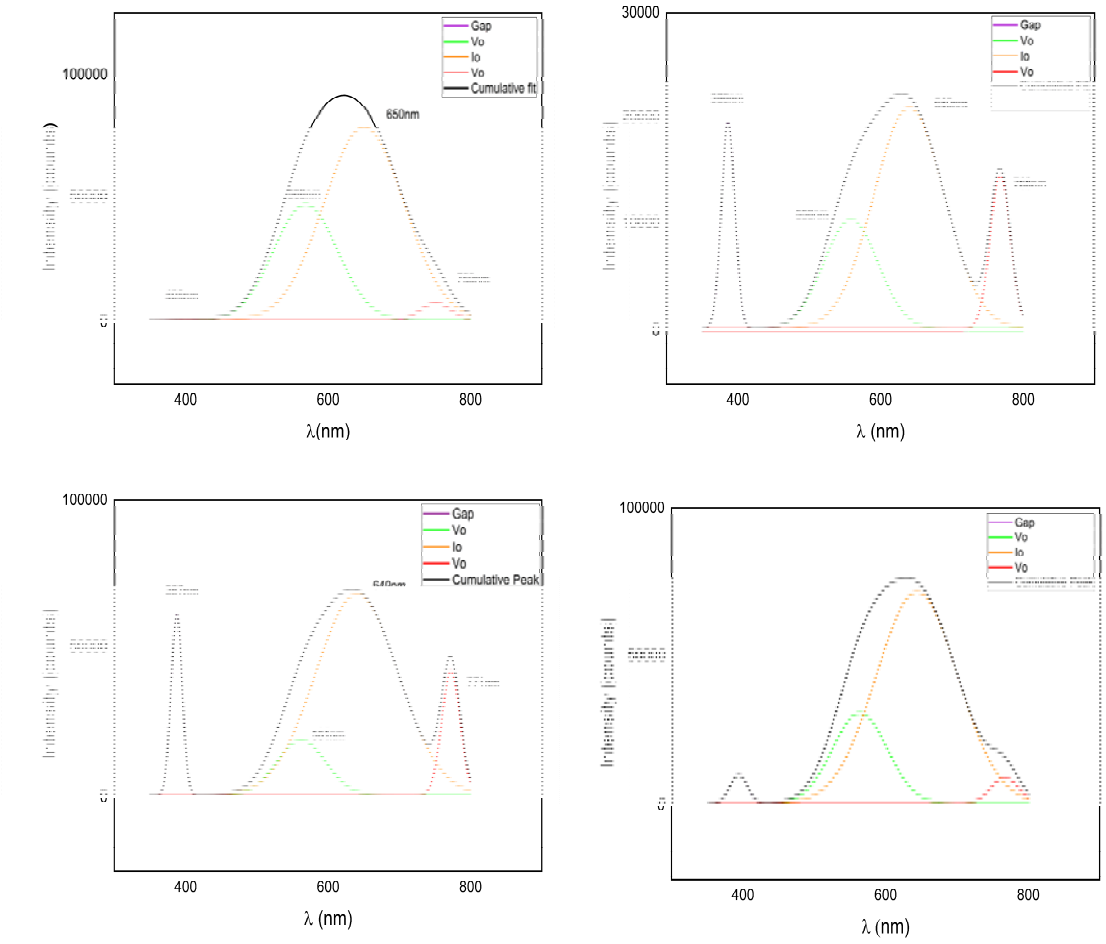

Figure 7: Photoluminescence spectra of Pepti, Polyol, NR and ND samples (top left to bottom right).

After deconvolution, the spectra show the same electronic transitions, in varying proportions, corresponding to the different defects present in the zinc oxide crystal structure, namely:

1. Transitions from the conduction band to the valence band (Gap);
2. Transitions from the conduction band to the oxygen defects (Vo),
3. Transitions from the conduction band to the interstitial oxygen (Io),
4. Transitions from the conduction band to another oxygen defects (Vo).

Electronic transitions associated with oxygen vacancies are of great importance for catalysis in the dark. Oxygen dissolved in water reacts with the electrons trapped in this vacancy to create a superoxide anion that can induce bacterial degradation reactions.

To get rid of the quantitative aspect of these oxygen vacancies, a comparison of the areas under the curves corresponding to the electronic transitions of the oxygen vacancies and the gap can be considered. The larger the ratio, the higher the amount of oxygen vacancies and the more efficient the catalyst should be.

Photocatalytic performances of the different synthesized powders were evaluated by the degradation of a model pollutant para-nitrophenol (PNP). For this purpose, test tubes were filled with 10 mg of the synthesized zinc oxide types and dispersed in 10 mL of a 10^{-4} M of PNP aqueous solution. They were placed around a halogen lamp, covering a spectrum from 350 nm to 800 nm. The lamp and tubes were kept at a temperature of 20 °C by a water circulation system.

In parallel, and in order to distinguish photocatalytic degradation of PNP from adsorption, duplicates of all tubes were made and placed in the dark.

The absorbance of the PNP solution was measured after 4, 8 and 24 h by withdrawing 1 mL of each PNP solution with a syringe and passing the solution through a 0.2 micron filter in order to remove any zinc oxide. The filtered solution was placed in a PMMA cuvette to which 2 drops of 0.01 M HCl were added to promote the acidic form of the pollutant. Measurements were done by using a UV-VIS spectrophotometer (Genesys 150 UV-VIS from Thermo Fischer Scientific) at a wavelength of 317 nm, which correspond to the acidic form of PNP with a maximum in the spectra at 317 nm. (Figure 8) Afterwards, the concentration of the remaining PNP was determined.

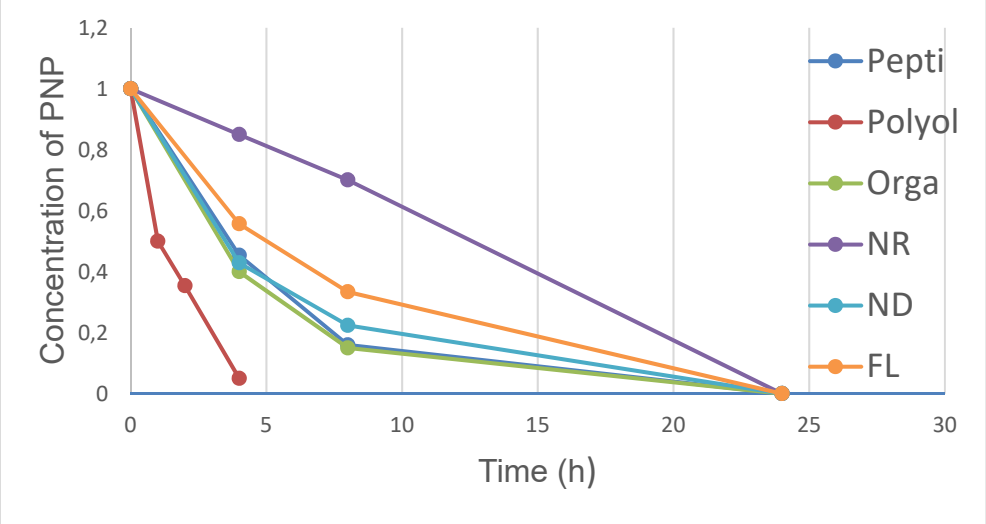

Figure 8: Degradation of PNP as a function of time for the different catalysts.

In order to understand whether certain radicals are more involved than others in the degradation of PNP, scavenger experiments were performed. Isopropanol was used as a hydroxyl scavenger and ammonium oxalate as a hole scavenger.
As it can be seen on the following Figure 9, the hydroxyl radicals play an important role in the degradation of the PNP.

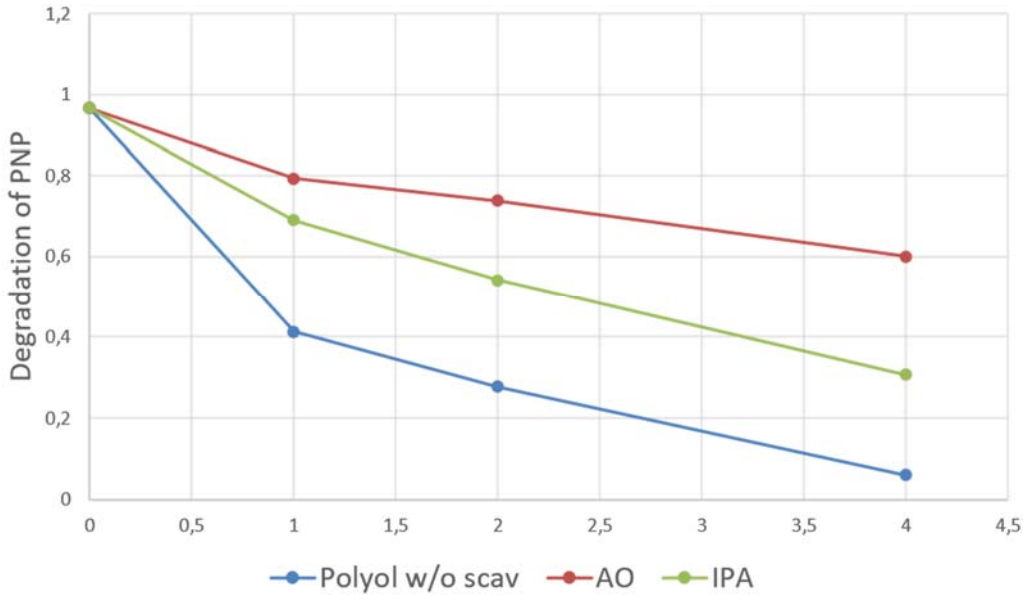

Figure 9: Scavenger experiment showing the degradation of PNP as a function of time for polyol catalyst.

Since the degradation of PNP leads to the formation of benzoquinone, a superoxide anion inhibitor, the effectiveness of PNP cannot be assessed by the use of this pollutant.
Moreover, since catalysis in the dark by oxygen vacancies only creates superoxide anions, it is preferable to use a dye that has an affinity for the latter. This was done by using nitro blue tetrazolium (NBT). The following Table 3 summarises the different degradation experiments carried out with the catalysts in the dark:

Table 3: Degradation of PNP in % in dependence of time to evaluate photocatalytic performance.

Catalyst/time of deg.	**24 h**	**48 h**
Pepti	10%	30%
Pepti NaBH4 (1)	30%	80%
Pepti NaBH4 (2)	40%	100%

3.2.2 Task 2.2: Development of antibacterial textiles

Various techniques exist in the laboratory, among which dip-coating appears to be the most appropriate solution for coating large filters.

In terms of the dip-coating process of the PA textile with the ZnO NPs, a total of 8 sets of experiments were carried out, with at least 50 individual experiments conducted altogether. The experiments included changing certain operating parameters of the dip-coater, changing the concentrations of the ZnO suspensions, and carrying out different methods to alter or activate the PA surface to promote further interactions with the ZnO NPs. As each set of experiments was developed, the approach of subsequent experiments was determined based on the results observed. All the experiments were carried out in triplicate.

The dip-coating process works by attaching the substrate to one of the clamps of the dip-coater, placing the suspension in a flask below the clamp and setting the required parameters for the motor to move as desired. The dip-coater has a simple set up and a limited amount of control parameters which allows for a relatively good control in terms of the reproducibility of the experiments (Figure 10 and Table 4).

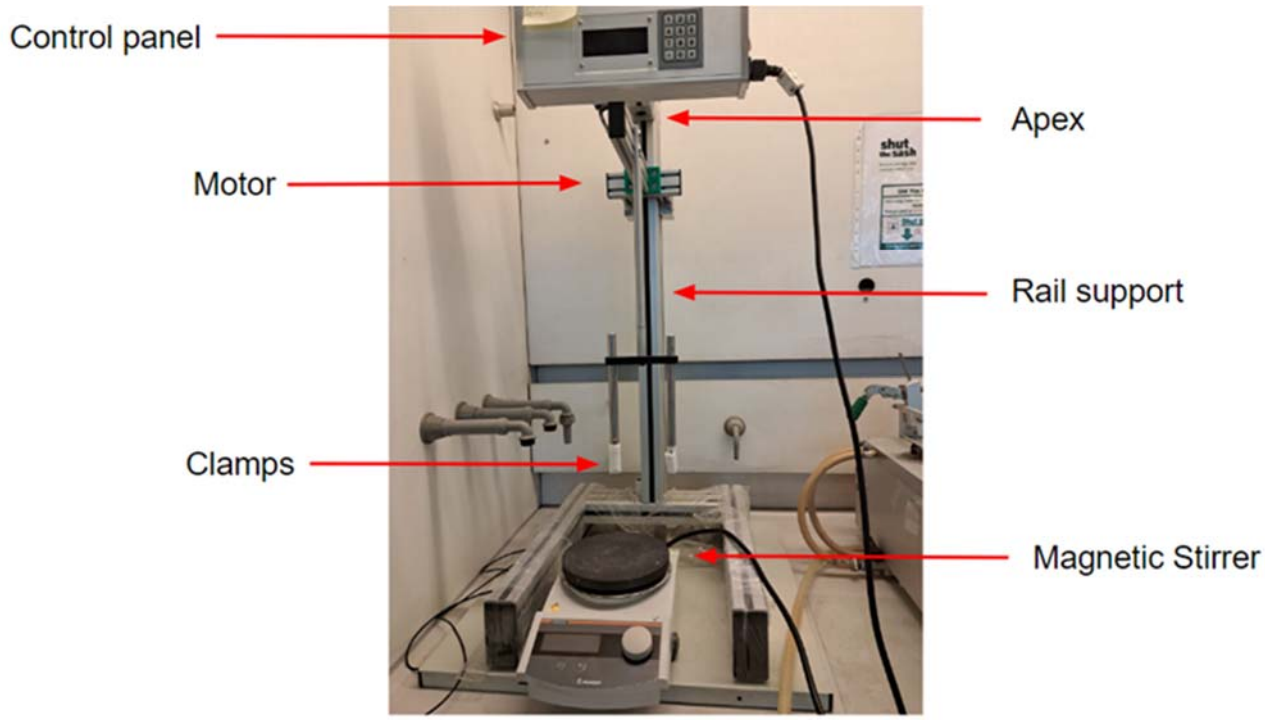

Figure 10: Experimental set-up for the dip-coater.

Table 4: Dip-coater control parameters.

Parameter type	Parameter	Unit	Description
Speed	Speed Down Distance	mm/min	The speed at which the motor moves downwards from the offset to the dip position.
	Speed Up Distance		The speed at which the motor moves upwards from the dipping position to the offset position.
Time	Time dip	min	The duration of the motor being in the dip position and the substrate remains submerged in the suspension.
	Time up		The duration of the motor remaining at the offset position between each dip iteration
Iterations	Iterations	#	The number of iterations a cycle is repeated.

A cycle in the dip-coater consists of the motor traveling along the rail from the offset position at the given speed to a “distance” position, then to a “dip” position, remaining during the set “Time Dip”, then traveling back up to the “distance” position and the offset position, remaining at the offset position during the set “Time Up”. Finally, it moves up to the top of the track and back down to the offset position.

A general procedure was followed for each of the experiments that was carried out:

1. The PA textile was cut into pieces of around 3 x 3 cm^2.
2. The pieces were placed in a flask and a washing agent was added. The flask was then placed inside an ultrasonic bath for 15 min. This was done to clean the PA surface and ensure that any contaminants were removed before coating.
3. The pieces were removed from the washing agent and placed in individual plastic petri dishes.
4. The petri dishes were then placed in a drying oven for 15 min at 60 ºC to avoid exceeding the glass transition temperature of PA 6 (Perkin Elmer, 2019)).
5. After drying, each PA piece was weighed. This weight was recorded as the initial weight**.**
6. The PA pieces were individually clamped to the dip-coater and dipped into the ZnO NPs suspension, using the specified parameters for each experiment.
7. Once the dip-coating was completed, the PA piece was removed from the dip-coater and placed back in the petri dish.
8. The petri dishes were again placed inside a drying oven for 15 min at 60 ºC.

9. Once dried, each PA piece was weighed again. This weight was recorded as the post-coating weight.
10. The PA pieces were then placed under a constant flow of running water for 10 s.
11. The pieces were placed back in the petri dishes and inside the 60 ºC drying oven for 24 hours to ensure that all the water molecules had evaporated from the surface.
12. The pieces were weighed again, and the weight was recorded as the post-wash weight.

Different parameters are then optimized, such as dipping time, washing agent, speed up, suspension concentration, activation of PA by acid and base treatment in order to increase the mass of ZnO coated on it.

The results obtained are summarized in Figure 11 for one of the developed ZnO.

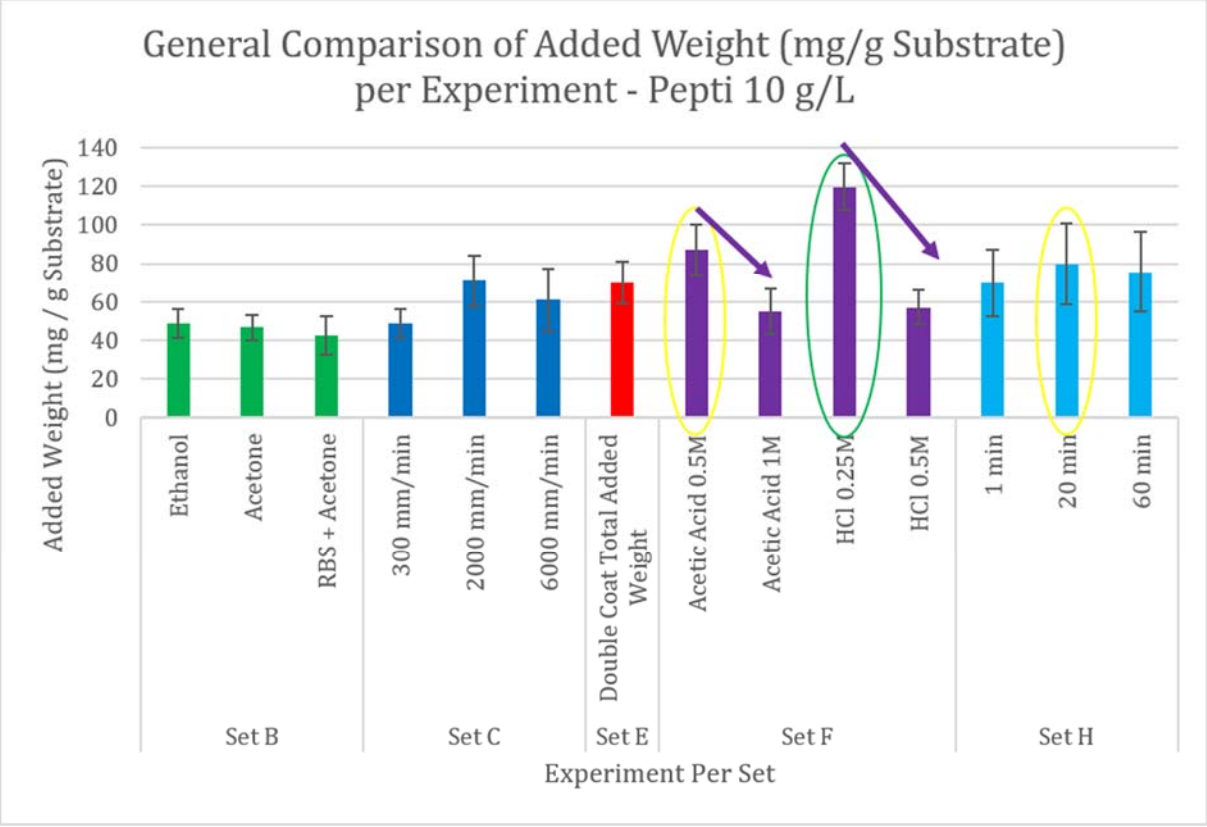

Figure 11: Results obtained for ZnO pepti with optimized parameters.

It can be seen that for both the acetic acid and the HCl, the weight of ZnO added decreases, as the concentration of the acids increases. In the case of the experiments conducted using the pepti suspension, the acid pretreatment experiments appear to be the only experiments that display any kind of noticeable pattern. Additionally, it can be seen that the highest added weight measured was achieved with the HCl 0.25 M pretreatment experiment.

Representative samples of some of the experiments performed were selected for characterization via SEM imaging. Figure 12 shows the images for each of the selected samples with a blank sample of the PA textile as a reference.

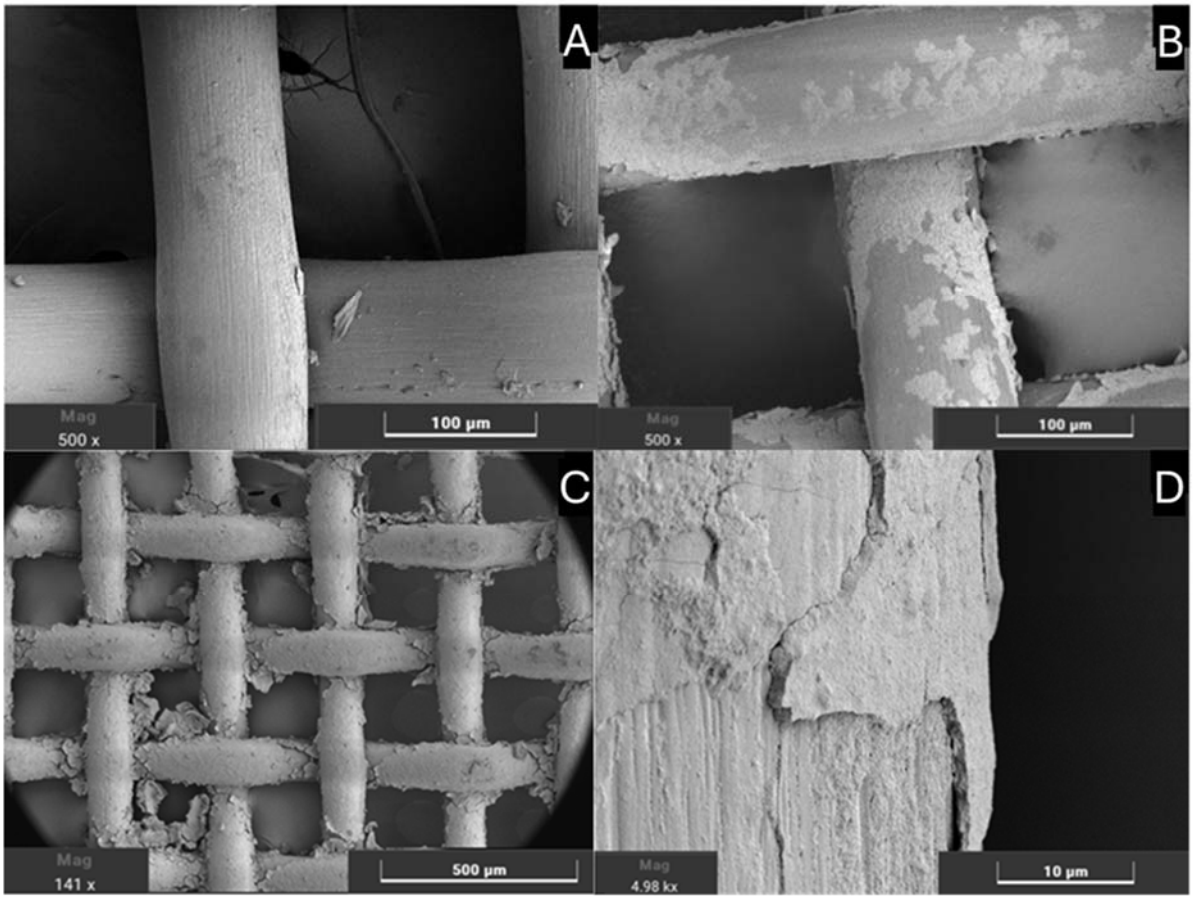

Figure 12: SEM images of textiles without ZnO (A) and with ZnO coated on it (B-D).

Further characterization methods (EDX) were performed on some of the samples, following the SEM imaging, to confirm that the substance observed coating the substrate was ZnO NPs (Figure 13).

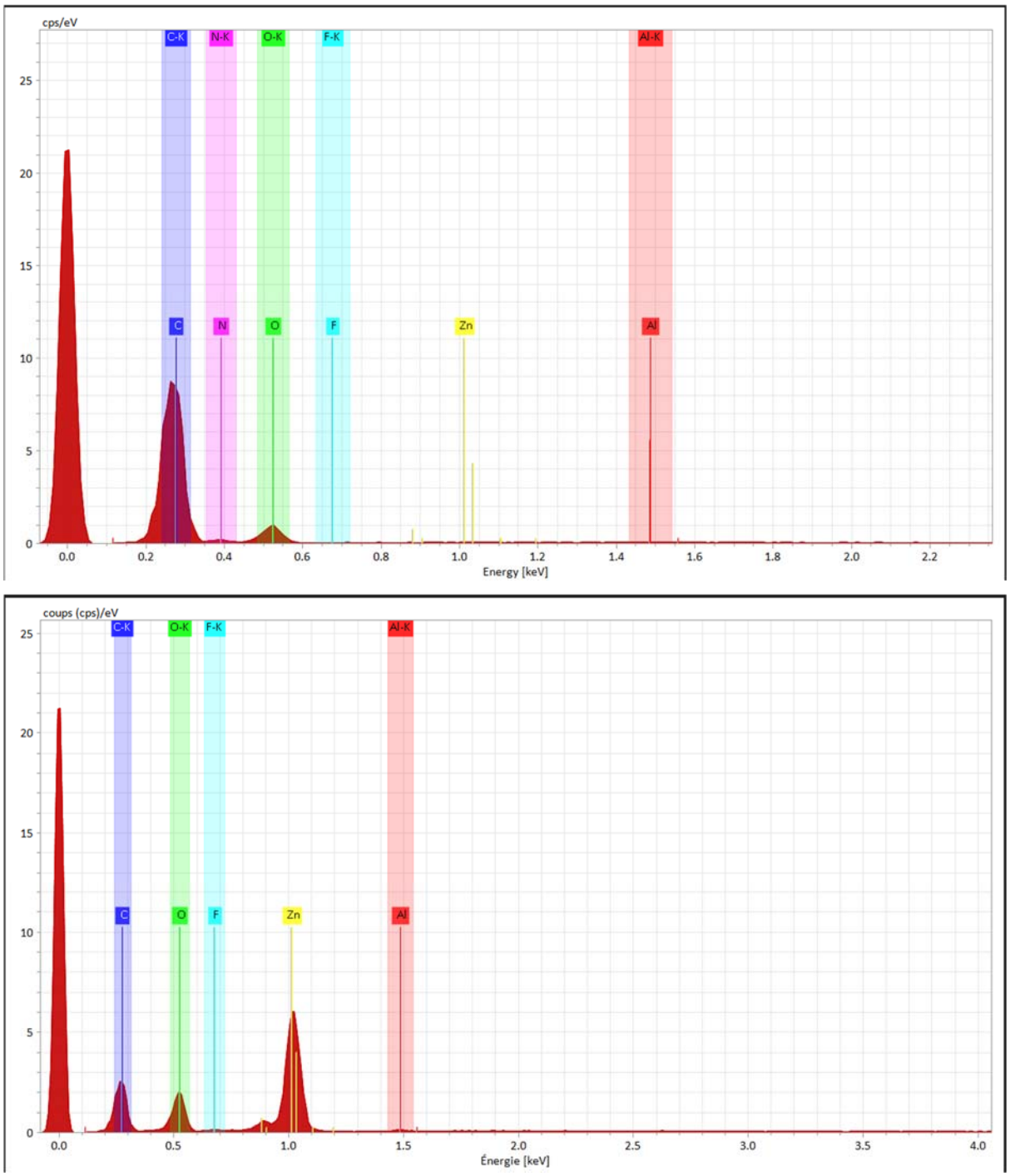

Figure 13: EDX spectra without (top) and with ZnO (bottom) coated on it.

3.2.3 Task 2.3: Analysis of antibacterial properties

Two types of antibacterial (AB) protocols were performed under sterile conditions in the bacterial hood. Tests were performed on 3 types of substrates; powders, textiles and 3D-printed filters modified with ZnO (Figure 14). The tests were first performed under UVA and then in the dark.

Test 1: AB Tests in the dark

- 100 mL of E. *coli* suspension 108 cfu/mL in a 500 mL Erlenmeyer flask.
- 6 h contact time powder-bacteria E. *coli* in the dark.
- Powder amount: 1 g/100 mL and 0.1 g/100 mL in Medium: 0.01 M NaCl.
- Control without substrate.

Test 2: AB Tests under UVA

- 100 mL E. *coli* suspension 108 cfu/mL.
- Contact time powder-bacteria E. *coli*: 1 h, 30, 20, 10 min under UVA LED UVA GdTech plate.
- Powder amount: 0.1 g/100 ml E. *coli* suspension in Medium: 0.01 M NaCl.
- Count on Petri dishes.
- Control without substrate.
- Sterilize 4 cristallizors with high edges, quartz plate, UV lamp, agitator under UVC light.

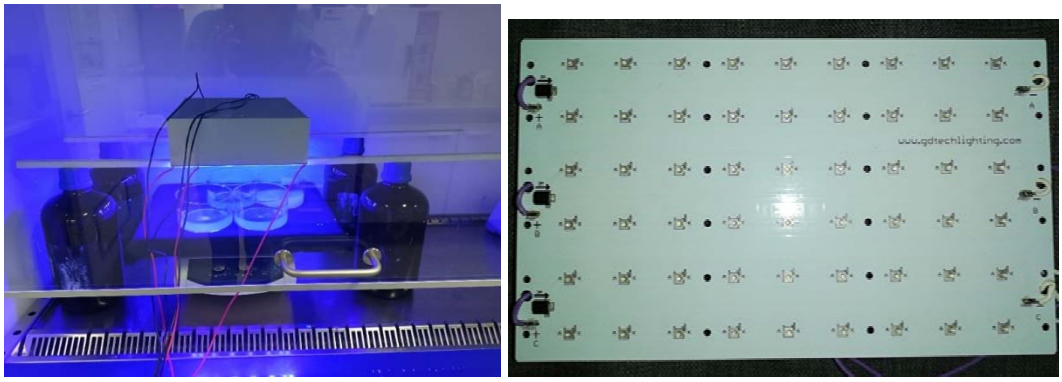

Figure 14: Experimental setup under sterile conditions and UVA (left) and the used UVA LED Lamp (right)

The first antibacterial tests were performed on powders synthetized by Uliege. Results are described in Table 5. A significant antibacterial effect (i.e. more than 2 log reduction) is observed after 1 h of UVA irradiation. In contrast, no antibacterial effect of the powder is observed in the dark after 1 h of contact.

Table 5: First antibacterial tests of ZnO powders performed in dark and in UV conditions.

Sample	Mass ZnO (mg)	cfu/mL
Control	0	4.05E+06
Pepti	102	2.00E+06
ZnO T	113	5.35E+06
Polyol	117	3.00E+06
Control UV	0	0.00E+00
Pepti UV	102	5.00E+02
ZnO T UV	113	5.00E+02
Polyol UV	117	5.00E+02

In the next experiments, the contact time between the powders and the bacteria was decreased to 30, 20 and 10 min. Three types of powders were tested under UVA irradiation. The results are listed in Table 6 and Figure 15. The figure highlights the bacterial degradation over contact time. It was shown that the different ZnO coatings increase E. *coli* degradation kinetics under UVA. This graph also highlights that the pepti and ZnO polyol coatings are the best candidates.

Table 6: Antibacterial tests of ZnO powders in suspension with different UV contact times.

Sample	Control (cfu/mL)	10 min UV (cfu/mL)	20 min UV (cfu/mL)	30 min UV (cfu/mL)
Control	1.70E+06	2.70E+06	2.35E+04	5.50E+03
Pepti	6.10E+05	0	0	0
ZnO	5.10E+06	3.00E+04	0	0
Polyol	6.20E+05	0	0	0

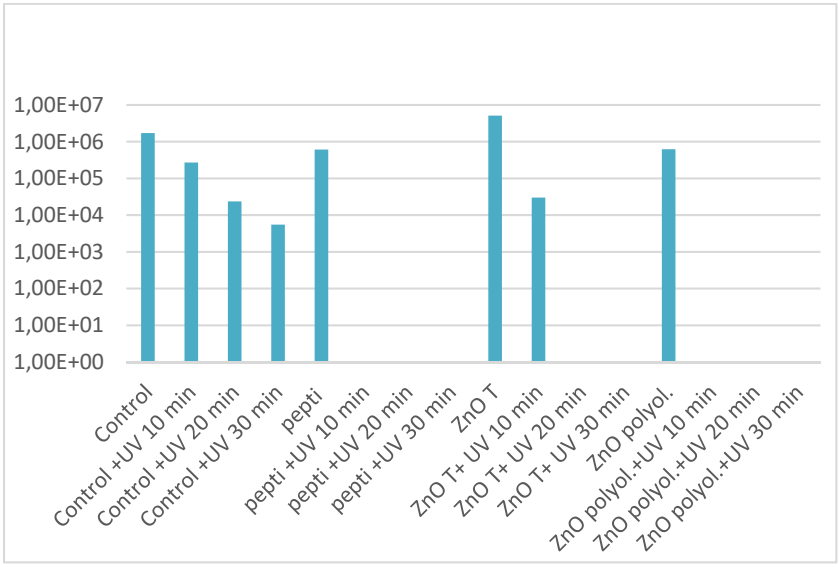

Figure 15: Antibacterial tests of ZnO powders in suspension with different UV contact times. Y-axis shows the cfu/mL of E. *coli*.

The next experiments were performed in the dark for 6 h. Results are described in Table 7 below. A significant antibacterial effect was observed with the different powders after 6 h of treatment in the dark.

The Zn leaching in the bacterial solution was also characterized in the bacterial suspension after the bacterial test. Significant Zn leaching was observed in the different solutions. The bactericidal effect seems to be correlated to the Zn leaching in the water.

Table 7:Parameters describing the antibacterial tests performed in the dark with a smaller selection of samples and tests on Zn leaching of the same samples.

Sample	ZnO (mg)	Number of bacteria (cfu/mL)	Zn leaching (mg/L)
Control	0	9.50E+10	
Pepti	104	6.05E+02	0.992
Polyol	108	5.35E+03	11.4

The next experiments were repeated in the dark for 6 h to confirm the results. Significant antibacterial effect was observed for the pepti coatings after 6 h of contact in the dark.

In addition, zone of inhibition experiments were carried out to test the microbial inhibition of certain reactants/chemicals/substances or materials. The zone of inhibition test, also known as disk diffusion test, assesses the sensitivity of microbial organisms to antimicrobial agents. For this test microorganisms are plated on an agar plate and the antimicrobial agent is applied in cavities in the agar or applied on thin paper plates and placed on top of it. The incubation

period is 24 - 48 h, depending on the bacteria, and their growth rate and conditions. The antimicrobial agent diffuses into the surrounding medium, inhibiting the growth of bacteria that are susceptible to the agent. As the concentration of the diffused agent decreases radially, at a threshold, bacteria can grow. Around the applied agent a clear circle can be seen, which is defined as the zone of inhibition of that agent. The diameter of the circle relates to its effectiveness. The zone of inhibition is measured with a ruler and reported in millimetres. In Figure 16 the principle of inhibition tests is shown.

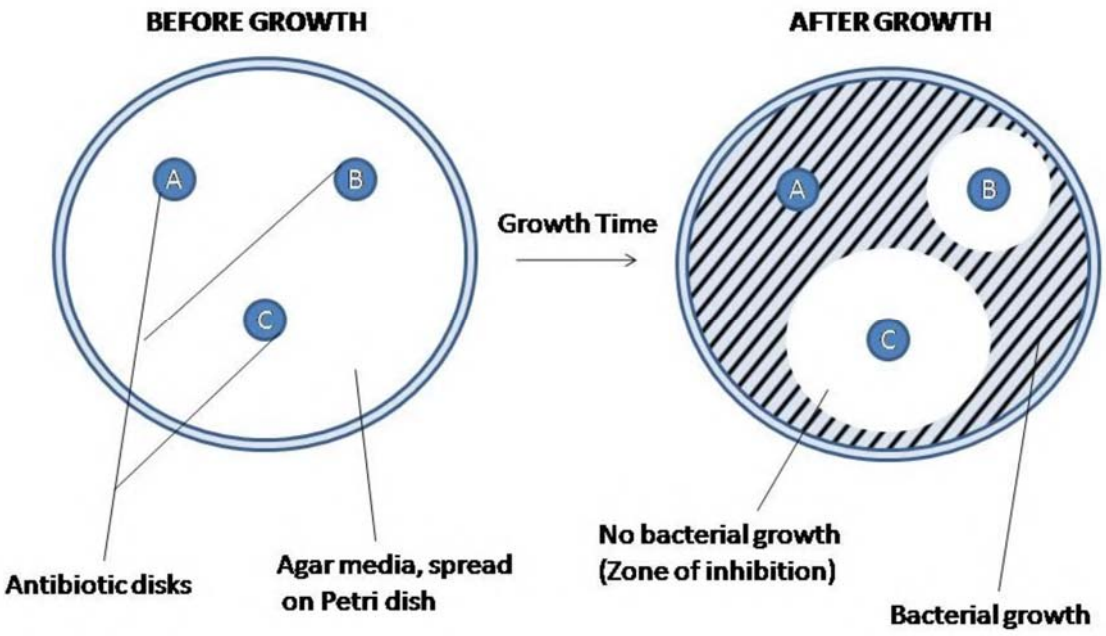

Figure 16: Sketch of a zone of inhibition test showing the plate before and after bacterial growth. Bigger zones of inhibition appear with greater inhibition of the substance.

This experiment was performed for the different selected ZnO's. As proof of concept, 1 mg/mL concentrated ampicillin (antibiotics) solution was applied as a positive control. Beyond this CuO and TiO_2 were tested. No significant inhibition was observed for TiO_2 and CuO. The strongest inhibition could be observed for the positive control.

DAF3D-1 and DAF3D-2 did inhibit the growth of B. Subtilis successfully with inhibition zones. of 20 mm. The zone of inhibitions can be seen in Figure 17.

Figure 17: Zone of inhibition for B. Subtilis for (clockwise) Ampicillin, DAF3D-1 and DAF3D-2, TiO_2 and CuO.

3.3 WP 3: Development of the antibacterial thermoplastics (IUTA)

WP 3 deals with the development of the antibacterial thermoplastics. In order to implement ZnO structures with antibacterial properties in thermoplastics, biocidal ZnO micropowders were first synthesized. These powders were then compounded with the thermoplastics using an extrusion process.

3.3.1 Task 3.1: Synthesis of biocidal ZnO micropowders

Following these tests, for the compounding with thermoplastics, the ZnO synthesis is focused on ZnO-A (pepti) and ZnO-B (polyol).

To synthesize ZnO-A, 5.9 g of zinc acetate dihydrate ($Zn(CH_3COO)_2.2H_2O$, VWR CHEMICALS, Netherlands) are dissolved in 250 mL at 80 °C, under stirring. At the same time, 4.5 g of KOH were also dissolved in 130 mL of ethanol. After dissolving each compound, KOH was added dropwise to the zinc acetate solution to react for 2 h and then washed three times with ethanol and oven-dried for 12 h at 100 °C to obtain a powder.

To produce the ZnO-B (polyol) zinc acetate dihydrate was dissolved in diethylene glycol ($C_4H_{10}O_3$. MERCK, Germany), to reach a concentration of 30 g/L of zinc oxide. Starting at room temperature, it is increased up to 140 °C to achieve complete dissolution. The temperature was then further increased to 180 °C, and the solution became opaque and white. The reaction took place during 2 h. The suspension was washed three times with ethanol and the resulting powder was oven-dried for 12 h at 100 °C.

3.3.2 Task 3.2: Compounding of thermoplastics with ZnO micropowders and development of the plastic filaments

The acquisition of the 3Devo Composer 450 allowed for simultaneous progression on WP3.2 and WP3.4. In the following text these tasks are described comprehensively. The workflow used for the compounding is according to material research papers. (Vidakis, 2022).

Before the compounding of any material can begin, the intended processing procedure is tested with pure polyamide 12 (hereafter PA12). The collected data is used to determine relevant parameters and optimize the extrusion process. PA12 is used in the form of a powder, which is a waste material from SLS processes. The powder is dried for 24 h at 80 °C to remove any moisture. The dried powder is then fed directly into the extruder (Figure 18). For the first experiments, a premade set of parameters was used. The parameters include temperature zones (H4 – H1), screw speed and cooling after extrusion.

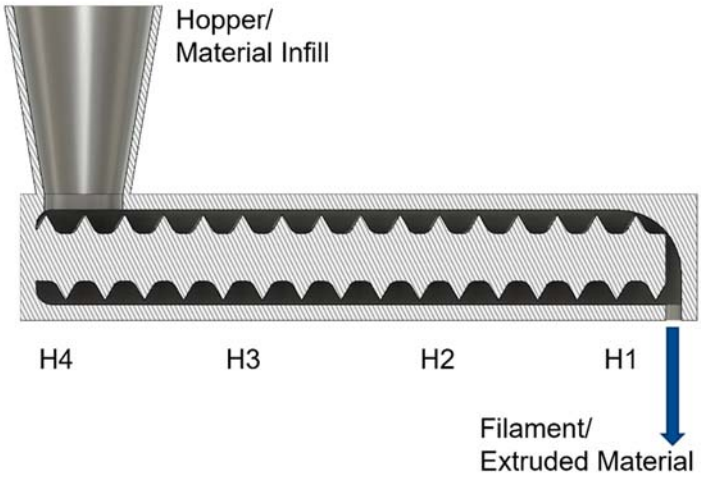

Figure 18: Sketch of the cross-section of a single-screw extruder. Design is based on the 3Devo Composer 450.

These parameters were then adjusted during the extrusion process until the resulting material had acceptable properties. These include the continuous filament thickness which must be 1.75 ± 0.1 mm. If the thickness could be maintained within the given tolerance (compare Figure

19), the next strand of material was wound onto a roll typical for FFF filaments. This completes the extrusion process of pure PA12 and the resulting filament is ready for use in 3D printing.

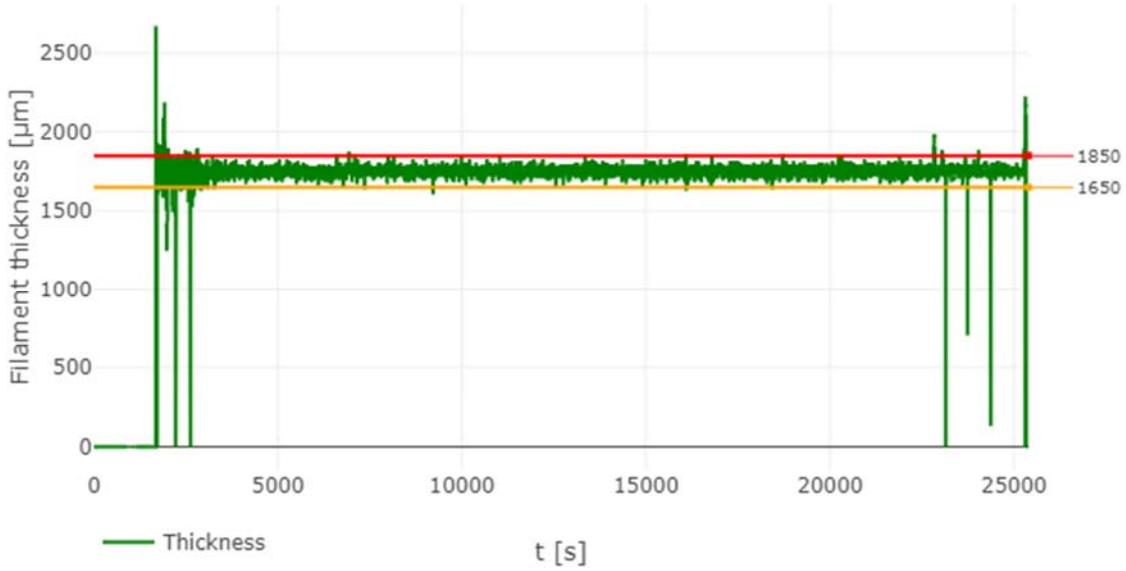

Figure 19: Diagram of the filament thickness over time. The value is only recorded during the process of spooling of the filament. Beforehand, the value is controlled until a consistent diameter is reached, so that spooling can begin.

Following the successful extrusion and winding of pure PA12, the compounding of materials was tested with ZnO-SA and followed by ZnO-DAF3D-1 and ZnO-DAF3D-2. Zinc oxide was added to the dried PA12-powder in ratios of 1-6 wt% of ZnO. Starting with 1 wt% blend and using the previously determined parameters, extrusion was performed, and the parameters were adjusted according to the new results. The process itself remained unchanged. After producing the 1 wt% compound, the obtained parameters were used and adjusted for the 2 wt% blend. This process was repeated up to the 6 wt% mixture (Table 8). After preparing the mixtures of one ZnO, the same procedure was applied to the next ZnO. Each mixture has a total weight of 100 g before processing. Losses were observed during the extrusion and winding. On average after weight loss, 30 m of filament of 1.75 mm diameter were obtained. The extruded materials were all winded to ensure their printability and to further test the 3D-printing properties (Figure 20).

Table 8: Parameters of extrusion which led to successful spooling of filament.

Compound	H4 (°C)	H3 (°C)	H2 (°C)	H1 (°C)	Rotation (rpm)	Cooling (%)
PA12	212	210	208	205	3.4	95
DAF3D-1 1 wt%	222	220	217	216	3.6	95
DAF3D-1 2 wt%	222	220	219	217	3.6	95
DAF3D-1 3 wt%	222	223	220	219	3.6	95
DAF3D-1 4 wt%	225	223	222	220	3.6	95
DAF3D-1 5 wt%	227	225	224	222	4.0	95
DAF3D-1 6 wt%	227	225	224	222	3.6	95
DAF3D-2 1 wt%	222	220	217	216	3.6	95
DAF3D-2 2 wt%	218	216	214	212	3.4	95
DAF3D-2 3 wt%	222	223	220	219	3.6	95
DAF3D-2 4 wt%	225	223	222	220	3.6	95
DAF3D-2 5 wt%	220	222	218	215	3.6	95
DAF3D-2 6 wt%	220	222	220	216	3.6	95

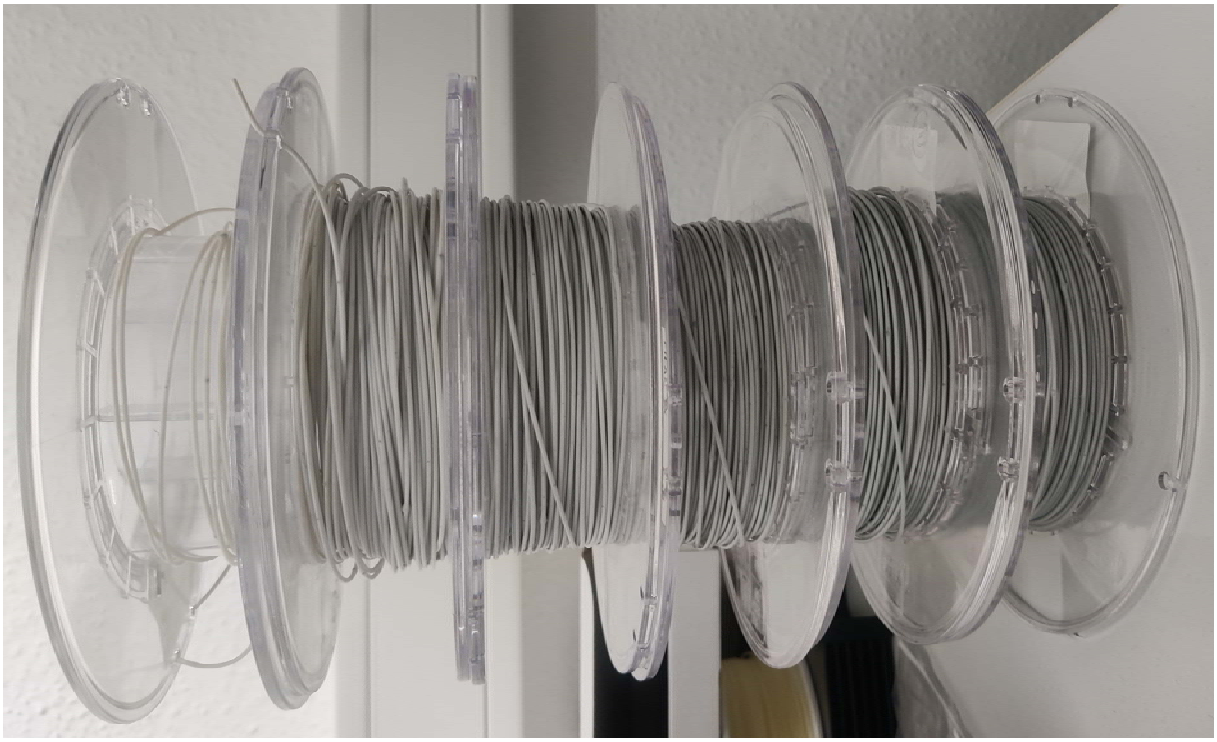

Figure 20: Extruded filaments of compounds with ZnO-DAF3D-2 by ULiège.

To test and verify the optimal printing conditions of the compounds, so called Temptowers have been printed. These are sample objects, which help visualizing several characteristics that are common causes of printing failure. These characteristics include bridging, overhangs, stringing, delamination, warping and breakage (Figure 21). A Temptower is created by stacking

several identical units, each printed at a different temperature (Figure 22). For this test the temperature is increased in 5 °C increments.

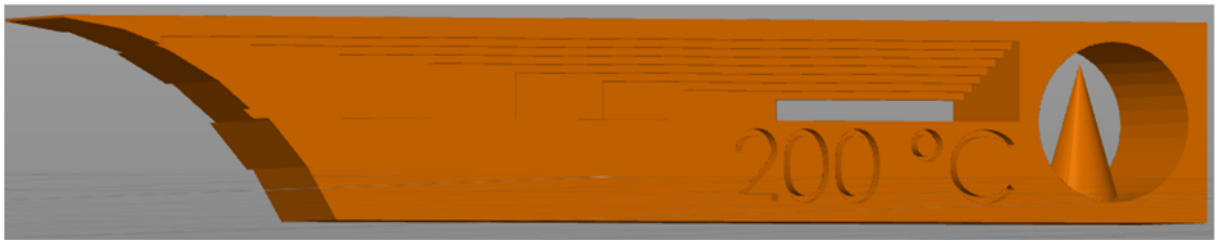

Figure 21: Unit of a Temptower. 10 x 10 x 100 mm³. Several characteristic typical for 3D-prints can be observed. Stringing at the cone on the right side. Bridges in the middle and overhangs at the left structure.

Again, starting with pure PA12 filament, the material was printed using standard PA12 settings. Most of the print settings were adjusted once and used unchanged for all compounds. Only the nozzle temperature range and the flowrate were changed as shown in Table 9 and Table 10.

Table 9: Parameters used for the 3D-printing of temptowers. Value ranges show changes during experiments.

Parameter	**Value**
Nozzle temperature (°C)	215 - 255
Printbed temperature (°C)	90
Layer height (mm)	0.2
Nozzle diameter (mm)	0.4
Infill (%)	30 - 40
Infill Form	Gyroid
Cooling (%)	75 - 80
Print speed (mm/s)	50
Layer count bottom	5
Layer count top	5
Layer count walls	2

Table 10: Parameters that were determined to result in successful printing specific to the compounds.

Material	Nozzle temperature (°C)	Flow (%)
PA12	230 - 245	100
SA 1 wt%	240 - 245	100
SA 2-3 wt%	240 - 250	100
SA 4-5 wt%	245 - 250	110
SA 6 wt%	245 - 250	110
DAF3D-1 1-3 wt%	240 - 250	110
DAF3D-1 4 wt%	245 - 255	110
DAF3D-1 5-6 wt%	no successful printing possible	
DAF3D-2 1-4 wt%	245 - 250	110
DAF3D-2 5-6 wt%	250 - 255	110

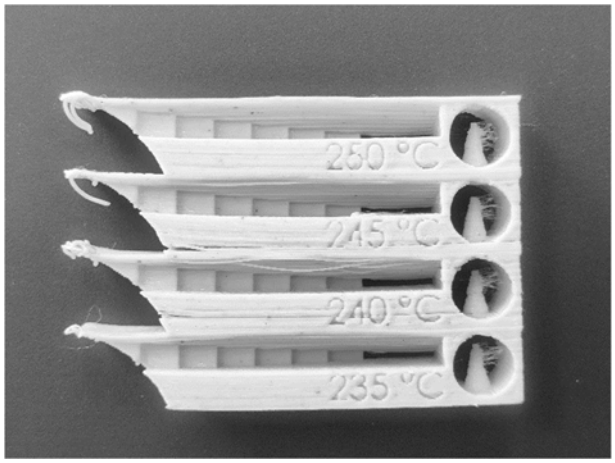

Figure 22: Printed temptowers of ZnO-DAF3D-2-2 wt% compound. Visible are layer separation at lower temperatures, stringing and sagging of filament in overhangs.

To verify the particle size of ZnO powders the method of dynamic light scattering (DLS) is used. 10 mL of distilled water was mixed with 1 mg of each ZnO powder and dispersed using an ultrasonic bath. 3 mL of the dispersion was then used for the DLS experiments. The results show peaks of light intensity at a particle size several times larger than expected (Figure 23).

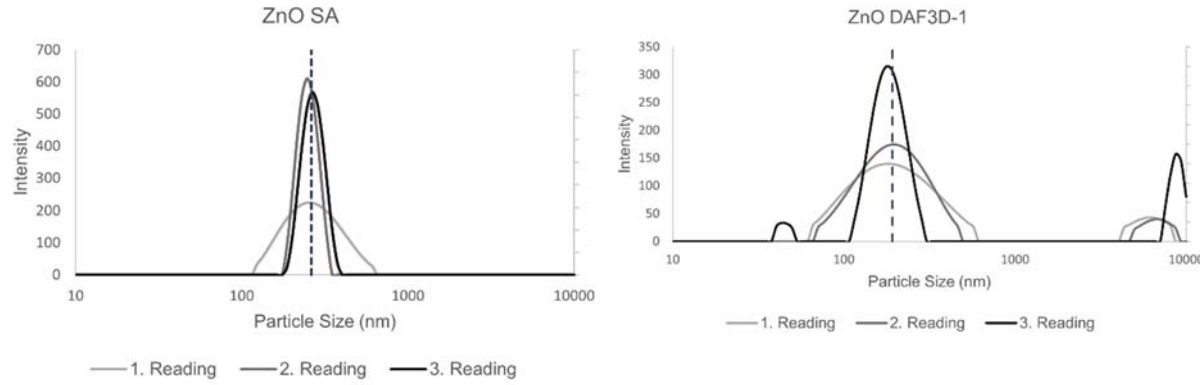

Figure 23: Mean particle size of ZnO-particles according to DLS method. The mean value is marked by a dotted line.

The particles were then characterised by analysing SEM images of the samples (Figure 24). Here, 1 µg of a powder was dispersed in 100 µL of distilled water. 20 µL of the sample was spread on a silicon wafer.

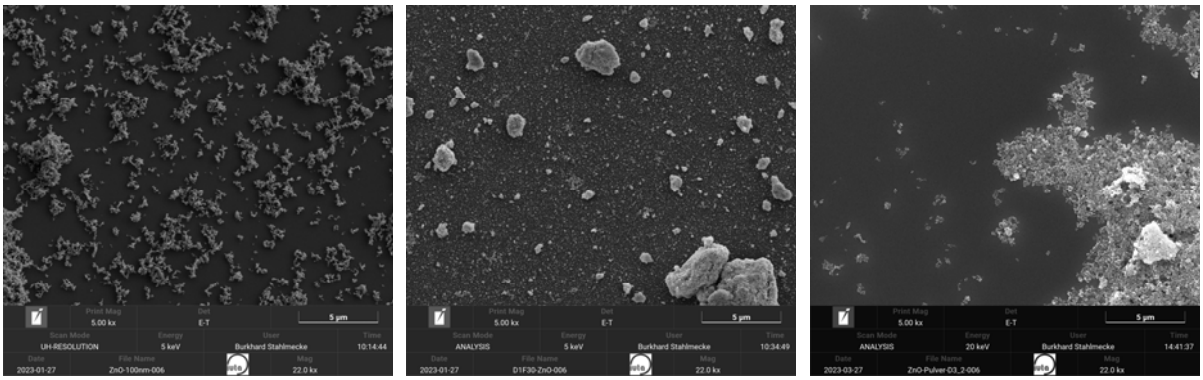

Figure 24: SEM images of ZnO particles (from left to right: ZnO-SA, ZnO-DAF3D-1. ZnO-DAF3D-2). Images taken at a magnification of 22 kx at 5 keV and 20 keV (far right).

The mean particle size was determined from these images and the result is closer to the expected values: SA 101 nm, DAF3D-1 is 27 nm and DAF3D-2 has a mean size of around 24 nm (Figure 25).

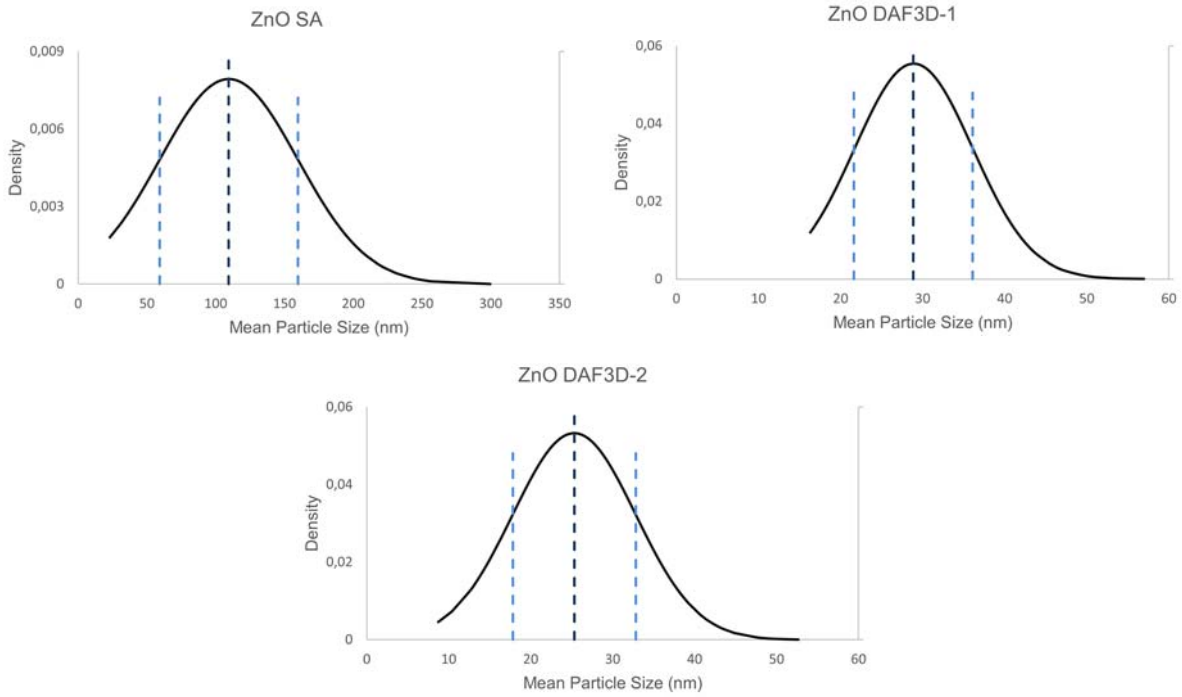

Figure 25: Mean particle size determined by SEM-analysis. The mean value and the first standard deviation are marked by dotted lines. Ca. 200 particles of each sample were measured.

Samples of the filaments were also prepared for SEM imaging (Figure 26). A 20 mm piece of filament was cut off and a 5 nm layer of gold was sputtered onto the surface. A control of pure PA12 was also prepared.

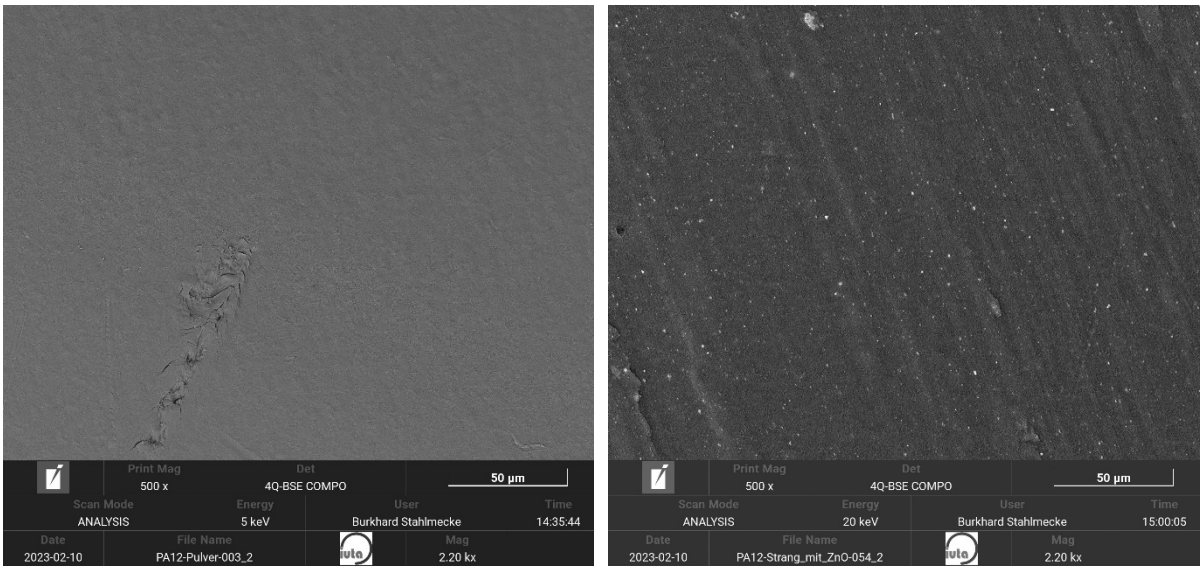

Figure 26: SEM images of filaments. Pure PA12 (left) and PA12-ZnO-SA-1 wt% (right). Images taken at a magnification of 2.2 kx.

The PA12 samples appeared to have a smooth surface with little to no disturbance. The compound samples in contrast showed white spots spread evenly distributed across the

surface. As these are not visible on the control sample, these are likely the ZnO particles. The size distribution of these bright spots was measured and compared for each compound (Figure 27).

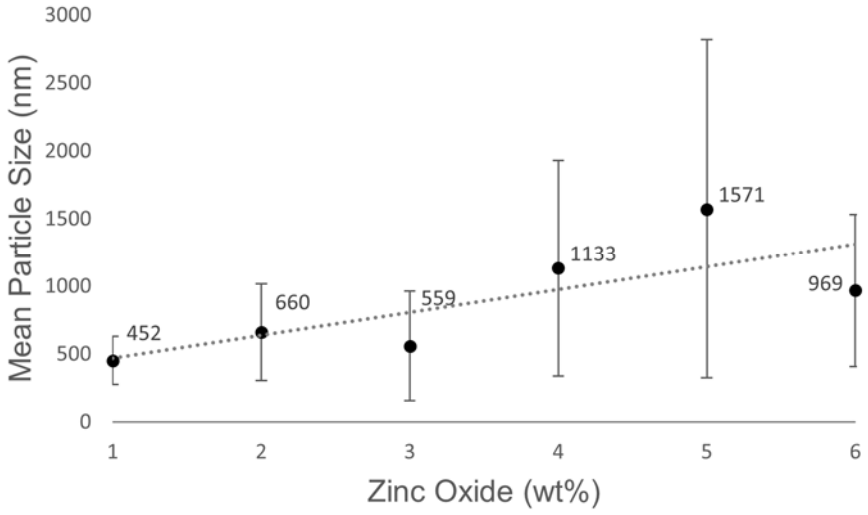

Figure 27: Mean size of agglomerations in ZnO-DAF3D-2 compounds as filament with 1-6 wt%. The respective mean values with their first standard deviation are noted.

The ZnO particles seemed to agglomerate and form larger agglomerations the higher the Zn concentration is.

After printing the temptowers, further samples were printed to be used in SEM analysis. Cylinders with a diameter of 14 mm and a height of 6 mm were produced (Figure 28 and Figure 29). These samples were sputtered with gold in the same way as the filaments.

Figure 28: Printed sample of PA12 used for SEM-analysis.

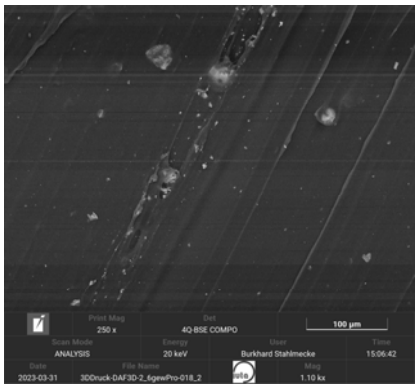

Figure 29: SEM image of printed sample at 1.1 kx magnification.

The same distribution as on the filaments was measured and is shown in the following Figure 30.

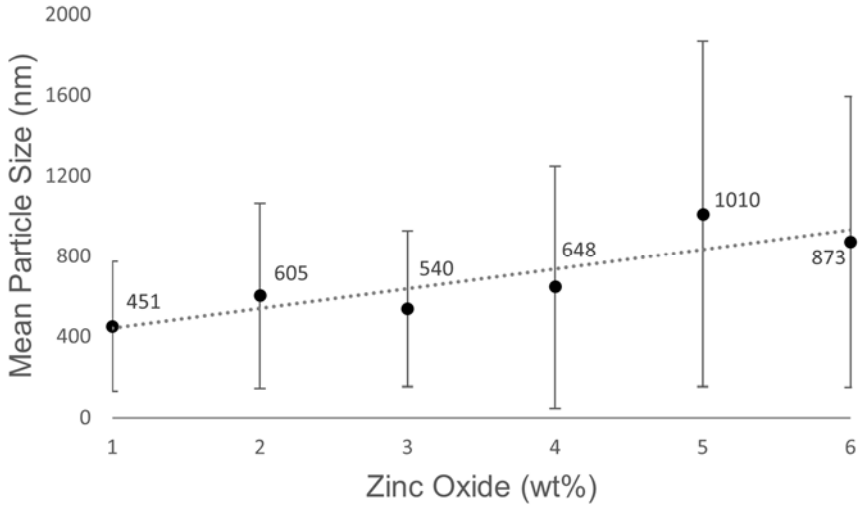

Figure 30: Mean size of agglomerations in ZnO-DAF3D-2 compounds as printed samples with 1-6 wt%.

As with the filaments the trend of agglomeration is similar. The comparison of the respective linear regressions shows a smaller mean size in the printed samples (Figure 31). This could be the result of the 1.75 mm thick filament being pressed through the printer nozzle which has a diameter of 0.4 mm and the extrusion at a height of 0.2 mm. Regardless of the cause the process of printing aids to evenly distribute the agglomerated ZnO in the printed samples.

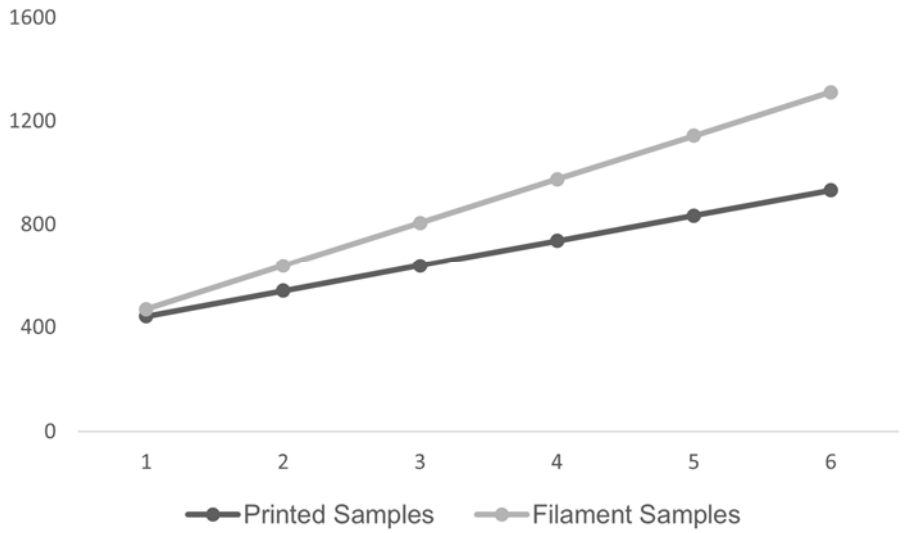

Figure 31: Linear regressions of the mean size of agglomerations in ZnO-DAF3D-2 compounds of filaments and printed samples in comparison.

3.3.3 Task 3.3: Antibacterial properties of the thermoplastics compounded with ZnO micropowders

In addition to the antibacterial tests on powders, tests were also performed on compounded filaments. These tests were done for 6 h in the dark with the E. *coli* bacteria. The bactericidal effect is low on the different filaments as seen in Table 11.

Table 11: Antibacterial and leaching tests on compounded filaments with the two synthesized zinc oxides. Shown are only the filaments with the highest concentration of ZnO.

Sample	cfu/mL	Zn Leaching (mg/L)
Control	2.94E+07	0
PA12	1.00E+06	0
PA12+Pepti 6wt%	1.00E+06	0.87
PA12+Polyol 6wt%	1.00E+06	0.91

Analysis of the inhibition zone of the compounded filaments and the corresponding additive showed no inhibition. It is assumed that the bioavailability of ZnO is not given when compounded with PA12.

It was assumed that a second heating step during 3D-printing would make the ZnO more bioavailable for bacteria. Therefore, 3D printed tablets were prepared to test the antimicrobial activity. To ensure that the tablets had maximum contact with the agar, they were slightly pressed into it. However, the printed tablets did not show microbial inhibition.

After the absence of antibacterial activity on the filaments, tests were repeated with powder blends with a higher proportion of ZnO particles. Results are shown in Table 12. The bactericide effect of the powders was confirmed, and Zn leaching was present.

Table 12: Antibacterial and leaching tests on powder mixtures with higher concentrations of ZnO.

Sample	Count of bacteria cfu/mL	Zn Leaching (mg/L)
Control	5.67E+07	0
PA12+Pepti 10 wt%	6.20E+02	5.9
PA12+Pepti 20 wt%	5.35E+03	7.3
PA12+Polyol 10 wt%	4.75E+02	5.4
PA12+Polyol 20 wt%	6.10E+03	3.3

3.4 WP 4: Necessary pretreatment of the different process waters (Celabor)

3.4.1 Task 4.1: Evaluation and Implementation of required pre-treatments

In most of the cases, the process water would have to be pre-treated before disinfection through the DAF3D filter. The aim of this step is to prevent soiling and clogging of the filter. Different pre-treatment steps were investigated depending on the process water composition (Figure 32).

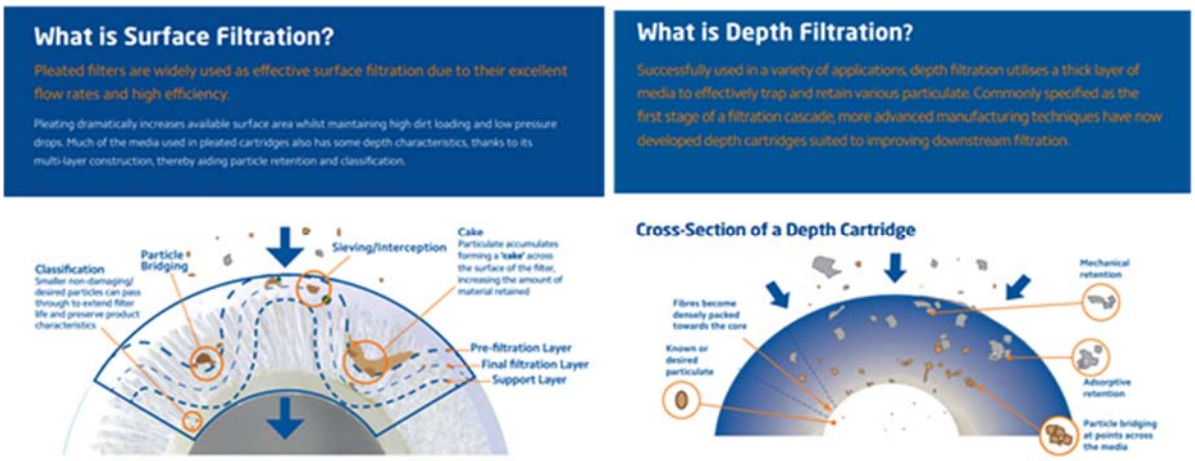

Figure 32: Sketches explaining surface (left) and depth filtration (right) (Celabor).

3.5 WP 5: Development and evaluation of the filter (IUTA)

As part of work package 5, a filter should initially be developed and manufactured for the installation of both coated textiles and the printed filter modules. Subsequently, tests should be carried out with real wastewater and model water to determine the antibacterial activity.

3.5.1 Task 5.1, 5.3: Dimensioning and development of the filter with antibacterial textiles and Task 6.1: Strengthening of the antibacterial activity of textiles

The filter design was adapted to the dimensions of the filters fitted with antibacterial textiles. A filter was divided into three modules of equal size and one of these modules was replaced by the textiles. The coated textiles were stacked to maximise the surface area and therefore the contact time.

For the following experiments additional filter beds were printed from virgin PA6 (Polyamide 6, Spectrum, Poland) and ASA (Acrylonitrile styrene acrylate, Fillamentum, Czech Republic), which were then coated with ZnO NP's instead of being compounded with ZnO. These materials did not require extensive parameter optimization as they were commercially available filaments.

For this task, ZnO pepti and ZnO polyol were used.

To coat the rather bulky filters, an impregnation technique was used, consisting of the following steps:

1. The filter is washed with ethanol;
2. A suspension of the ZnO under consideration is prepared at different concentrations;
3. The filter is immersed in the solution for 30 min;
4. The filter is removed and oven-dried at 60 °C for 1 h;
5. Steps 3 and 4 are repeated three times;
6. The filter is washed with deionized water and placed in the oven overnight.

A comparison with commercially available filaments was not made, because all available materials are not suitable regarding the material demands required by this project. Wastewater can reach high enough temperatures to potentially deform PLA and degrade it over time. The other materials, CPE and TPU, are not suitable due to their elastomeric properties.

3.5.2 Task 5.2: Development of the filter module

The filter construction is based on a mathematical model which is called triply periodic minimal surfaces (TPMS). This is a group of functions (1-3) of which each describes a 3-dimensional surface which is infinitely repeatable in every cartesian axis without any discontinuities. (Jung and Torquato, 2005; Thomas et al, 2018; Hesselmann, 2021; Feng, 2022)

Gyroid $$f(x,y,z) = cos(x) * sin(y) + cos(y) * sin(z) + cos(z) * sin(x) \quad (1)$$

Diamond $$f(x,y,z) = sin(x) * sin(y) * sin(z) + sin(x) * cos(y) * cos(z) + cos(x) * sin(y) * cos(z) + cos(x) * cos(y) * sin(z) \quad (2)$$

schwarz-p $$f(x,y,z) = \cos(x) + \cos(y) + \cos(z) \quad (3)$$

The first step to construct a filter module from these surfaces is to create a usable 3-dimensional surface from a function. The program called MathMod (ver. 11.1), which can create object files, was used. These object files are further modified in the program Blender (ver. 3.5). The surface is multiplied along the cartesian axes to create a 3-dimensional mesh of the TPMS. This surface mesh is then given a thickness to create a solid body. This new mesh is then cut into the shape of a cylinder with a diameter fitting to the test tubes (42 mm) for the following experiments. Several different structures were tested (Figure 33). The constructed filter samples were exported as stl files for use in the slicer program for the printing process. Chosen for printing were a diamond TPMS, a gyroid TPMS, a schwarz-p TPMS, and a conventional mesh which was constructed in Blender as well.

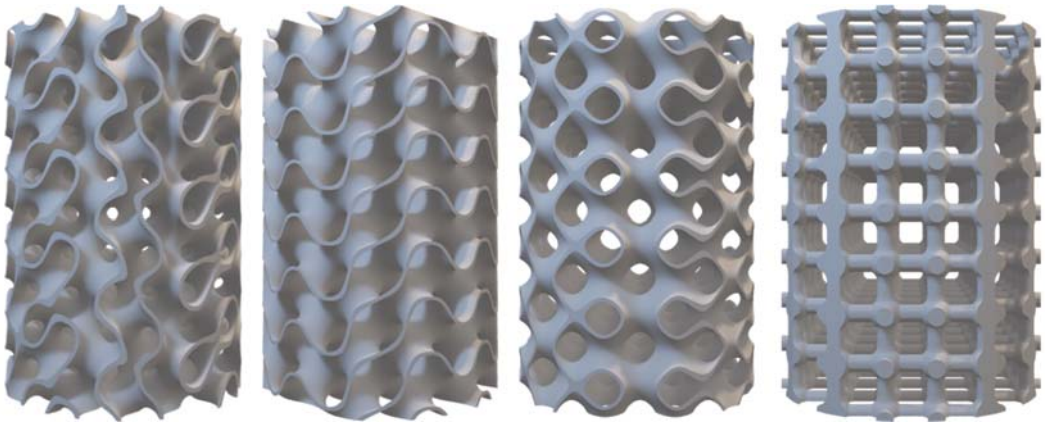

Figure 33: 3D-models of the tested filter meshes. From left to right: gyroid, diamond, schwarz-p, and a generic mesh construction, which finds use typically in such structures.

These filter bed samples with their specific structure were 3D-printed using pure PA12 as material to test the viability of the structures. A Creality Ender 3 S1 and the software CrealitySlicer (ver. 4.8.2) were used. Due to the material showing warping and adhesion issues, modifications were made to the construction and the printing settings obtained from the temptowers. The design modifications include a 64 mm diameter brim on the bottom layer and a realignment of the mesh along the z-axis. The parameters of the printing process were also modified, as the parameters previously used for the temptowers could not be used to

achieve a successful print of this size and complexity. The layer height was reduced to achieve a high vertical resolution and print quality, the print speed was reduced, and several changes were made to reduce stringing and warping in the print. Other changes are listed in Table 13.

Table 13: 3D-printer settings used for the printing of the filter module.

Category	Parameter	Value	Unit
Quality	Nozzle Size	0.4	mm
	Layer Height	0.12	mm
	Line Width	0.44	mm
	Initial Layer Height	0.24	mm
Material	Bottom Pattern Initial Layer	Concentric	
	Printing Temperature	232	°C
	Build Plate Temperature	68	°C
Speed	Print Speed	60	mm/s
	Initial Layer Speed	20	mm/s
Travel	Retraction Distance	2.4	mm
	Retraction Speed	35	mm/s
	Retraction Extra Prime Amount	-1	mm^3
	Retraction Minimum Travel	0.7	mm
	Maximum Retraction Count	0	
	Minimum Extrusion Distance Window	0.7	mm
	Combing Mode	All	
	Max Comb Distance With No Retract	50	mm
	Travel Avoid Distance	4	mm
	Z Hop Height	0.2	mm
Cooling	Enable Print Cooling	Off	

With this adjusted set of parameters, the different structures were printed (Figure 34 and Figure 35). The gyroid and diamond units could be printed with a good surface quality. The schwarz p unit was difficult to print successfully due to its internal structure necessitating a lot of bridging, which resulted in a comparatively poor print quality.

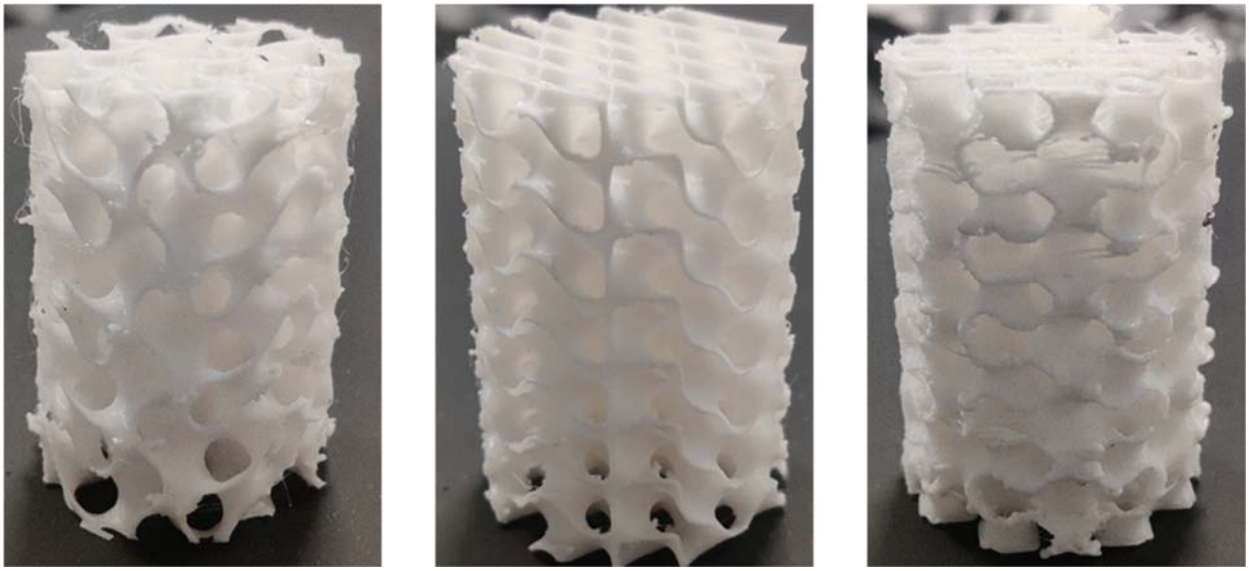

Figure 34: Printed TPMS-filter beds, from left to right: gyroid, diamond, and schwarz-p. Pure PA12. Cylinders have a diameter of 34 mm and a height of ~43.6 mm.

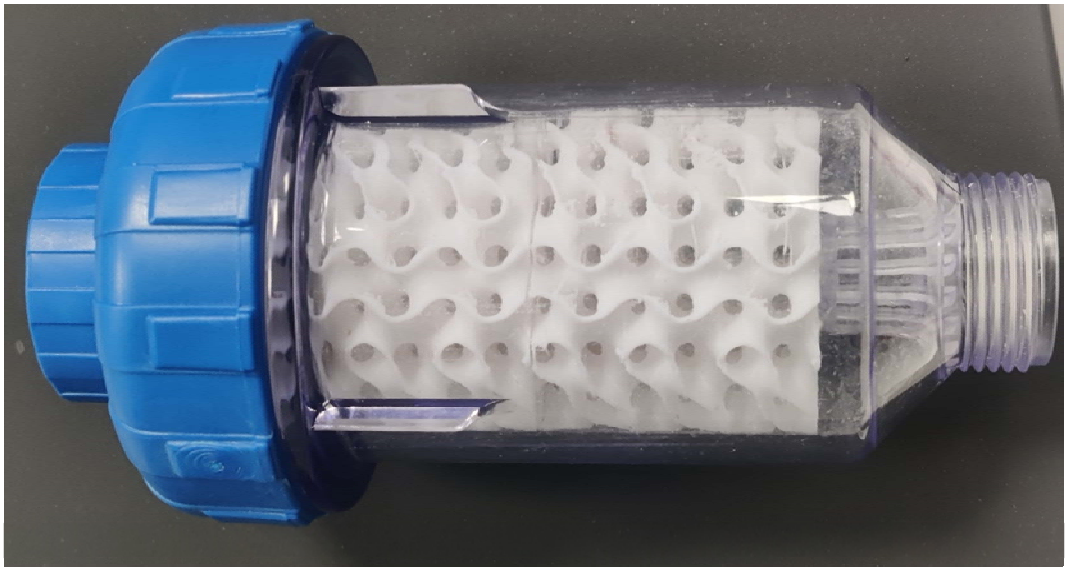

Figure 35: Printed gyroid filter bed encased in filter housing. Made from pure PA12. Printed in two parts for a total dimension of 70 x 42 mm.

3.5.3 Task 5.4: Examination of the filters with industrial process waters

Due to the higher contamination of process water with organic and inorganic components and the associated greater influence parameters on the filters, the planned tests with industrial process water were postponed.

3.5.4 Task 5.5: Analysis of antibacterial properties

To quickly determine the antibacterial activity of the filters, they were operated with diluted nutrient solution containing B. subtilis. At the same time, a test was carried out with an uncoated filter. The filter speed was 5 m/h and the flow through the filters was from top to bottom. In Figure 36 the results of experiments over a time period of 0.5 h and 2 h are given. The thermoplastic used was ASA. The coating was polyol. The control filter (blue line) was uncoated (Figure 36).

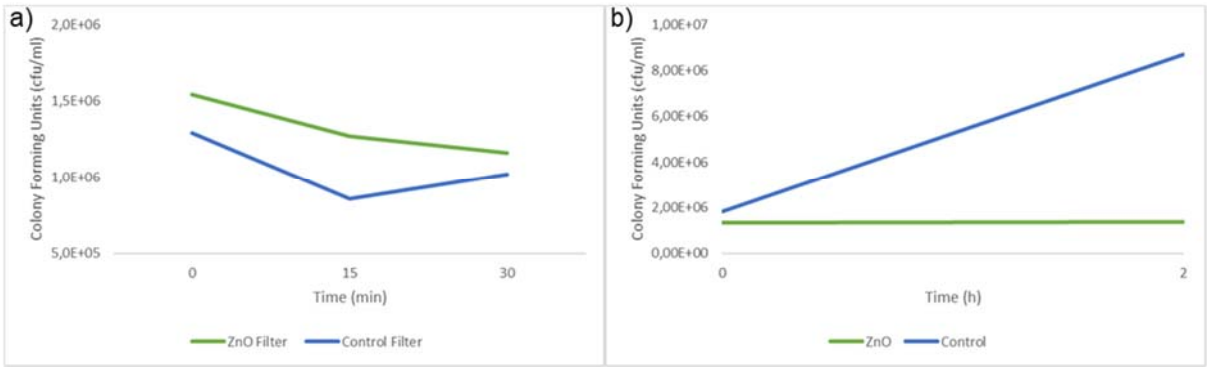

Figure 36: Count of bacteria during an a) 0.5 h and b) 2 h experiment (Thermoplastic: ASA, coating: polyol).

3.6 WP 6: Optimisation of operating parameters for the demonstrator (ULiege-NCE)

To optimize the filters, an attempt is made to increase the antibacterial activity. The operating parameters of the demonstrator are also being optimized.

3.6.1 Task 6.1: Strengthening of the antibacterial activity of textiles

WP 6.1 was processed together with WP 5.1 and 5.3. The results are presented in Chapter 3.5.1.

3.6.2 Task 6.2: Optimization of the demonstrator

In the first series of tests it was observed that the filter chambers were not completely filled with water. As a result, the flow direction of the filter was inverted and the water eluted from bottom to top. In addition, the antibacterial activity of the filters was very low at a filter speed of 5 m/h, so it was reduced to 1 m/h. In addition, the test duration was adjusted to extend the contact time. The filter properties and operating parameters are summarised in Table 14.

Table 14: Properties and operating parameters for each filter module.

Parameter	Unit	Value
filter bed height	m	0.07
width of the filter	m	0.042
filter bed volume	m^3	0.000097
filter bed volume	L	0.0970
empty bed contact time	h	0.07
Filter speed	m/h	1
flow rate	mL/min	23
bed volume per hour	-	14

3.6.3 Task 6.3: Analysis of antibacterial properties of the demonstrator

Finally, antibacterial tests were performed on the 3D-printed filters. The contact time was 6 h in the dark. Results are described in Table 15. Less than 2 log of reduction was observed after 6 h of contact.

Table 15: Antibacterial and Zn leaching tests of ZnO coated 3D-printed filters with E. *coli*.

Sample	ZnO (mg)	ZnO (wt%)	Count of bacteria (cfu/mL)	Zn Leaching (mg/L)	Zn Leaching (%)
Control	0	0	2.10E+07	0	0
PA6 Polyol	127	1.65	3.50E+05	28	24
PA6 Pepti	83.2	1.09	3.50E+05	30	34
ASA Polyol	66	0.07	3.50E+05	42	64
ASA Pepti	40	0.56	3.50E+05	32	80

Further tests were conducted with B. *subtilis* and a contact time of 4 h (Figure 37).

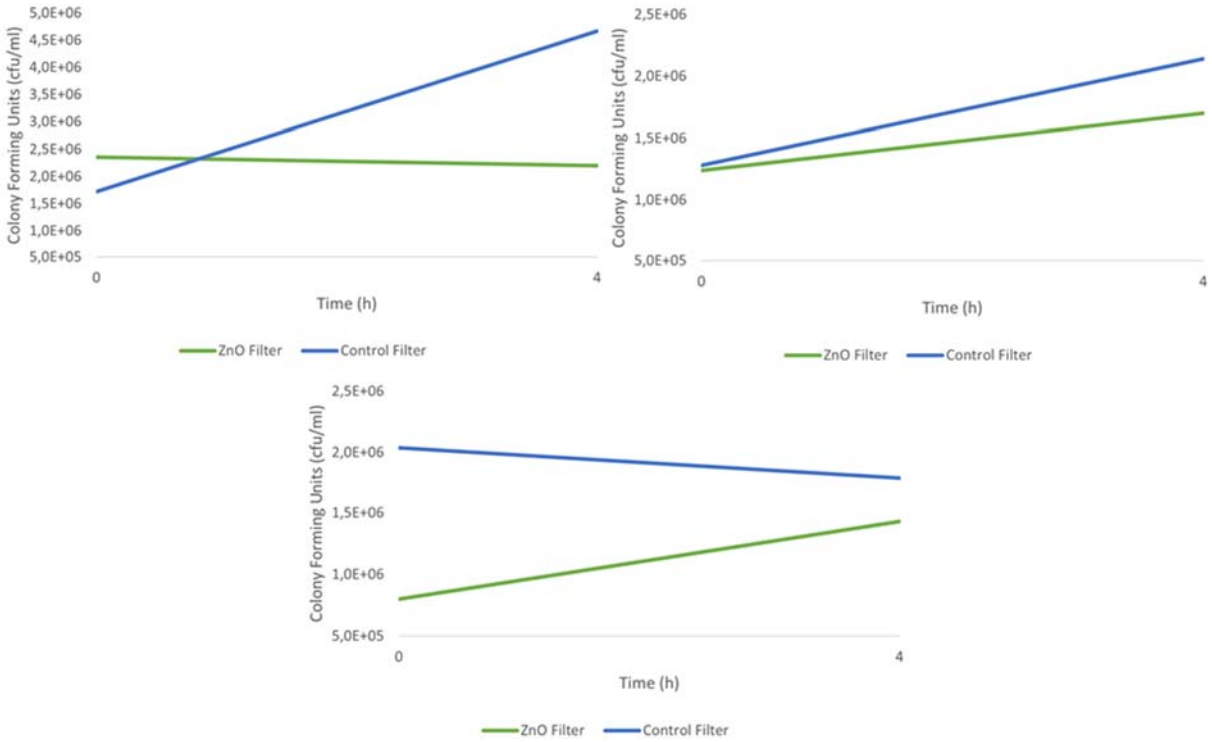

Figure 37: Antibacterial tests of ASA-Polyol (70 mg, 0.98 wt%), ASA-MeOh (74 mg, 1.03 wt%), PA6-MeOh (88 mg, 1.15 wt%) (in that order).

The tests were repeated in the same manner with coated textile filters fitted in between two purpose-made pieces of the printed filter (Figure 38).

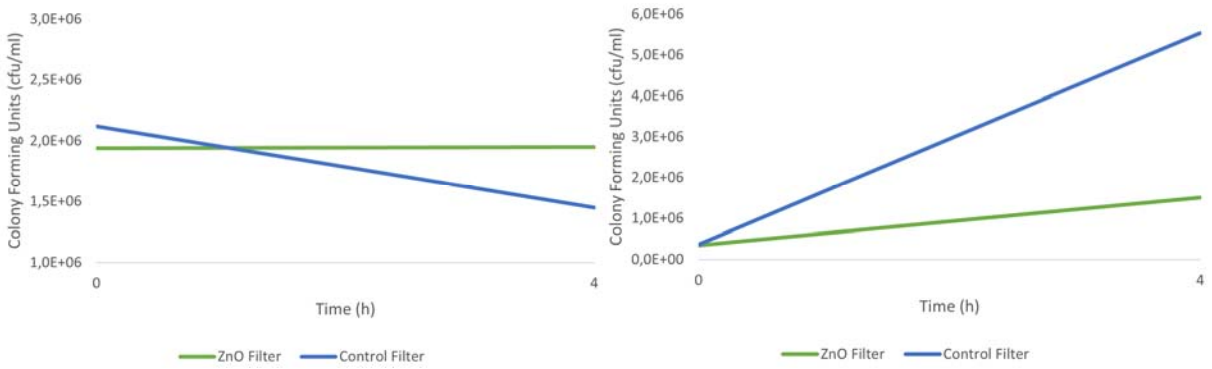

Figure 38: Antibacterial tests of Textile (PA66)-Polyol (left) and Textile (PA66)-MeOh (right).

Following these tests, a combination of the most efficient printed filter and textile was tested with a contact time of 5 days (120 h) (Figure 39).

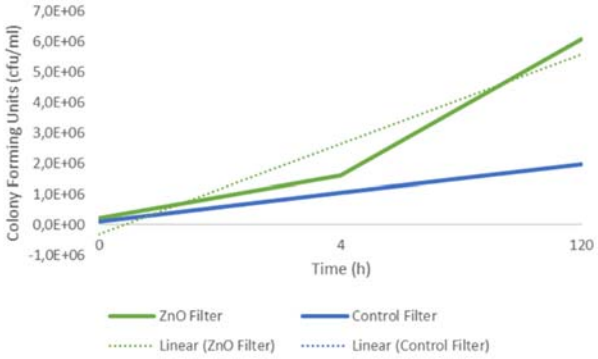

Figure 39: Tests of the mixed filter made from the printed ASA-Polyol filter and the textile-Pepti filter.

3.7 WP 7: Long term investigations (Celabor)

Within WP 7 long term experiments should be carried out on the filter demonstrator to investigate the durability of antibacterial properties on this module.

3.7.1 Task 7.1: Analysis of antibacterial properties

The ongoing antibacterial effect of the ZnO-added filter was to be demonstrated in a long-term test. To this end, a test was carried out for a period of 120 hours. Samples were taken after 0; 4; 24; 96 and 120 hours. The results were given in Figure 40.

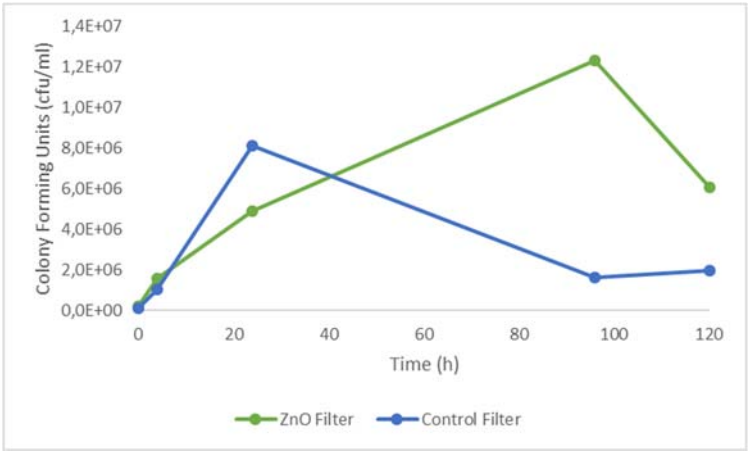

Figure 40: Illustration of the growth of the two filters (control = blue and ZnO filter = green) over the long-term test of 120 hours.

Strong bacterial growth was observed after just 4 hours, although growth was significantly stronger in the control test. Growth in the ZnO filter was delayed, but significantly stronger than in the control filter. In the control filter, after the growth phase and reaching the plateau after 100 hours, the bacteria already appear to be in a new growth phase after the death phase. In the ZnO filter, the death phase is only reached after 100 hours. A delay in growth could

therefore be achieved by the addition of ZnO. Accordingly, the filter showed a bacteriostatic and not an antibacterial effect.

However, Zn was also detected in the aqueous phase of the medium in parallel with the growth. After 120 hours, the concentrations in the experiment with ZnO were 8.8 mg/L. It is therefore unlikely that ZnO could be stabilised on the filter in the long term. This led to the cancellation of the experiment.

3.7.2 Task 7.2: Investigations of AOC and NTS

The Non-Target screening (NTS) led to the following results. The overview of the features and their correspondence across the different analysis replicate groups are shown by the chord plot below (Figure 41). Overall, there is an increase in the number of features as the experiment progresses, but these are mainly unique in each analysis replicate group. This indicates that the unique features are related to chemicals being formed and degraded. Metabolites from biological activity could explain the dynamic change in features, occurring with the highest intensity after 24 h for the control (without ZnO) and after 120 h for the test with ZnO. Possibly, the presence of ZnO delayed and slightly mitigated the biological growth when comparing the test set with the control.

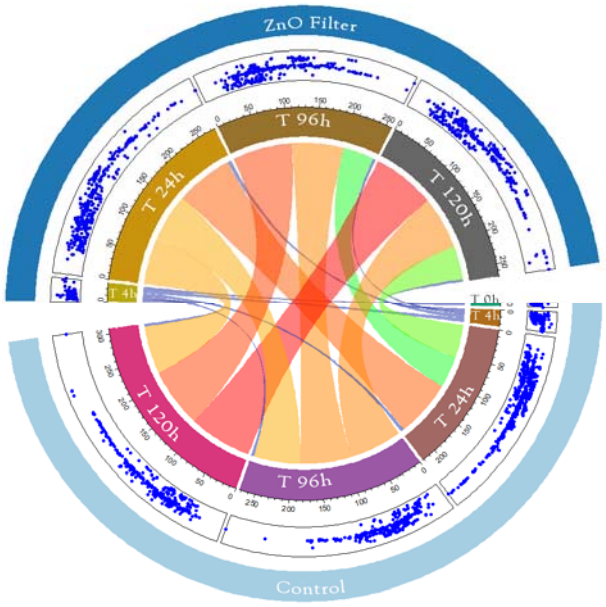

Figure 41: Shown in this chord plot are the aforementioned features analysed by NTS and how they overlap between the different samples.

The results of the assimilable organic carbon (AOC) also reflect a similar picture (Figure 42). The AOC indicates the proportion of total organic carbon that can be directly metabolised by

bacteria. In the control filter, the concentration of AOC after 120 h was approx. 750 and in the ZnO filter approx. 1,000 µg/L.

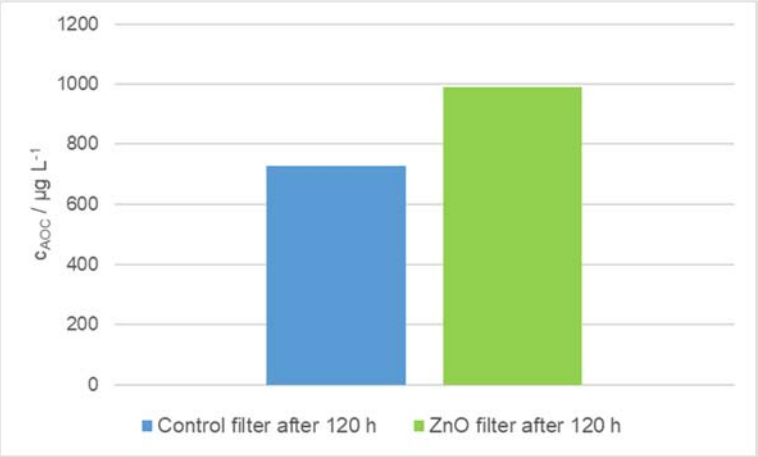

Figure 42: Concentrations of the AOC after 120 h for the control filter (blue) und the ZnO filter (green).

3.8 WP 8: Dissemination (IUTA; ULiege-NCE; Celabor)

In addition to the regular meetings of the project committee and the project partners, the results were presented to a wide audience at national and international conferences in the form of poster presentations, lectures and publications.

3.8.1 Task 8.1: Dissemination and use

An oral communication titled “Development of antibacterial functionalized textiles by 3D printing” was presented in «NANO 2022 – 16th International Conference on Nanostructured Materials», in Sevilla (Spain), from 6 to 10 June 2022, and in “EDT-MAIN PhD Scientific Day / NanoWal annual meeting”, in Namur (Belgium), January 31st 2023.

A poster titled “Development of antibacterial functionalized textiles by 3D printing” was presented in “PREPA 13 – 13th International Symposium”, in Louvain-la-Neuve (Belgium) from 9 to 13 July 2023.

A poster titled “Entwicklung neuer antibakteriell funktionalisierter Textilien und 3D-gedruckter Filter für die Prozesswasseraufbereitung (DAF3D)“ was presented at the SUK (Spurenstoffe und Krankheitserreger im Wasserkreislauf) 2023 in Frankfurt am Main, Germany, 27.-28.03.2023.

A brief description of the project with initial results was published in the conference proceedings of SUK 2023 of DECHEMA (Gesellschaft für Chemische Technik und Biotechnologie e. V.) from page 63 onwards.

A scientific article is accepted for publication in “Journal of Sol-Gel Science and Technology, Special Issue: Photocatalytic materials by sol-gel processing”. The authors are Antoine Farcy,

Stéphanie D. Lambert, Dirk Poelman, Zetian Yang, Nathalie Body, Pierre Eloy, Sophie Hermans, Patrick Drogui, Benoît Heinrichs, Cédric Malherbe, Gauthier Eppe, Alexandre Verdin, Julien G. Mahy, and is entitled “Influence of crystallographic orientation of sol-gel ZnO on the photocatalytic degradation of p-nitrophenol in water”.

Another publication is in submission in the “Journal of Photochemistry & Photobiology, A: Chemistry”. The authors are Antoine Farcy, Julien G. Mahy, Christelle Alié, Joachim Caucheteux, Dirk Poelman, Zetian Yang, Pierre Eloy, Nathalie Body, Sophie Hermans, Benoît Heinrichs, Stéphanie D. Lambert, and is entitled “Kinetic study of p-nitrophenol degradation with spherical zinc oxide nanoparticles prepared by sol-gel methods”.

4. Conclusion

The synthesis of textile fibres coated with ZnO particles was successfully completed. Additionally, the bactericidal effect of the textiles was characterized. A significant bacterial reduction was observed with more than 2 log reduction of E. *coli* bacteria in the dark after 6 h of contact. However, this bactericidal effect is connected with a significant release of zinc.

The process of compounding thermoplastics with additives itself is well understood and was successfully completed in this project. By compounding thermoplastics with ZnO particles, a homogeneous distribution of ZnO particles was observed. The leaching of ZnO from compounded filaments was also significantly lower than for coated filaments.

The problems start to arise at the manufacturing step of 3D-printing. Materials with a high level of additives prove to be difficult to print due to the alteration of properties. In addition, PA is generally difficult to print and several issues, including the continuous stringing of the material, limited the regulation of pore sizes of the filter and other parameters regarding the construction of the module. The use of ASA lifted some of these limitations and would allow for more customization, for example the implementation of smaller pores and a higher specific surface area. The issue here is the compounding step due to the sparse amount of material sources. The construction of the filter module itself produced a satisfactory result, with a customizable object, able to fit a given set of criteria.

The two sub-goals of the project were successfully completed independently of each other. However, the combination of the synthesized ZnO with antibacterial properties without an additional UV source and the antibacterial effect of the printed filters could not be carried out satisfactorily. The use of PA12 demonstrated a homogeneous distribution of the ZnO particles throughout the filaments and test prints could be achieved, but no antibacterial activity was observed.

Long-term experiments also showed an insufficient antibacterial effect. The tests with industrial process water were not carried out as part of the project.

5. Presentation of the scientific-technical and economic benefits of the results obtained, in particular for SMEs, as well as their innovative contribution and industrial application possibilities

As part of the project, the synthesis of active ZnO species, which have an antibacterial effect without exposure to UV light, was successfully realised.

Another aspect of the project was the compounding of thermoplastics with different additives. This was successfully demonstrated in the project for various multi-component systems (thermoplastic + additive). A homogeneous distribution was achieved.

These extrusion processes thus made it possible to modify or change the properties of thermoplastics. By adding additives, for example, the durability of the thermoplastics can be improved. As part of the project, this was received with great interest, particularly among SMEs involved in 3D printing. During the project, however, it turned out that various thermoplastics are not commercially available in powder form. For this reason, it was not possible to evaluate the property changes for 3D printing for the thermoplastic ASA. Further research in the field of materials science and additive manufacturing is therefore necessary to bring the developed material to market maturity. It should be noted that the compounding of thermoplastics in particular offers almost inexhaustible potential for achieving special properties. The general feasibility has been clearly demonstrated.

Another area of research within the project was 3D printing with the thermoplastics produced in-house with the addition of additives. This was also successfully realised as part of the project. However, depending on the thermoplastic, the addition of a high percentage by weight of additive can have a significant negative effect on the printing properties.

6. Updated plan for the transfer of results to the economy

6.1 Information of the companies of the Project Monitoring Committee

As part of the project, the meetings accompanying the project were held online. The first two SME meetings took place as a combined Belgian and German event. The final event was held in mid-December 2023 in German for the German SMEs. The project-supporting committee consisted of plant manufacturers, research institutes from the fields of textiles and water research, sensor manufacturers and engineers.

6.2 Targeted addressing of potentially interested companies also outside the SME meetings

In addition to the SME meetings, other members of the project support committee were informed by telephone/email.

Both during the course of the project and after its completion, important conferences and trade fairs were and will be used to inform other potentially interested companies about the project content and results. This measure was also implemented by means of numerous advisory meetings at the research institution.

6.3 List of all transfer measures carried out and those planned beyond the project duration

The presentation of the results during the project period was mainly in the form of publications, lectures and posters at conferences, trade fairs, seminars and regional sector-specific events. Information on the chronological sequence of these transfer measures can be found in Table 16.

Table 16: Transfer measures of the DAF3D project.

Date	Measure	Description
28.01.2022	Kick-off meeting	
06.-10.06.2022	Oral presentation	NANO 2022 – 16th International Conference on Nanostructured Materials, Sevilla, Spain Title: “Development of antibacterial functionalized textiles by 3D printing”
14.06.2022	Project meeting	Presentation and discussion of the project results and further coordination, online.
22.09.2022	Project meeting	Presentation and discussion of the project results and further coordination, online.
17.11.2022	Project meeting	Presentation and discussion of the project results and further coordination, online.
16.01.2023	Project meeting	Presentation and discussion of the project results and further coordination, preparation international SME meeting, online.
31.01.2023	Joint SME meeting	Information of the SME committee, critical discussion of the work
31.01.2023	Oral presentation	EDT-MAIN PhD Scientific Day / NanoWal annual meeting, Namur, Belgium Title “Development of antibacterial functionalized textiles by 3D printing”

Date	Measure	Description
21.03.2023	Project meeting	Presentation and discussion of the project results and further coordination, preparation international SME meeting, online.
27.-28.03.2023	Poster presentation	SUK (Spurenstoffe und Krankheitserreger im Wasserkreislauf) 2023 in Frankfurt am Main, Germany Title: "Entwicklung neuer antibakteriell funktionalisierter Textilien und 3D-gedruckter Filter für die Prozesswasseraufbereitung (DAF3D)"
24.04.2023	Project meeting	Presentation and discussion of the project results and further coordination, preparation international SME meeting, online.
04.05.2023	Joint SME meeting	Information of the SME committee, critical discussion of the work
27.06.2023	Project meeting	Presentation and discussion of the project results and further coordination, online.
09.-13.07.2023	Poster presentation	PREPA 13 – 13th International Symposium", in Louvain-la-Neuve (Belgium) Title: "Development of antibacterial functionalized textiles by 3D printing".
22.08.2023	Project meeting	Presentation and discussion of the project results and further coordination, online.
07.-09.11.2023	IUTA Innovation Days	Possibility to visit the extruder and the 3D printers and exchange of project results
23.11.2023	Project meeting	Presentation and discussion of the project results and further coordination, preparation international SME meeting, online.
14.12.2023	Final SME meeting of the German SME committee	Information of the SME committee, critical discussion of the work
Accepted publication		Journal of Sol-Gel Science and Technology, Special Issue: Photocatalytic materials by sol-gel processing, "Influence of crystallographic orientation of sol-gel ZnO on the photocatalytic degradation of p-nitrophenol in water".
Submitted publication		Journal of Photochemistry & Photobiology, A: Chemistry, "Kinetic study of p-nitrophenol degradation with spherical zinc oxide nanoparticles prepared by sol-gel methods"

6.4 Assessment of the feasibility of the proposed and updated transfer concept

In the previous sub-chapter, the individual transfer measures were identified. This shows that numerous measures have been taken by the research institution to reach a broad public. IUTA has a large interdisciplinary scientific network and collaborates intensively with small and medium-sized enterprises within the framework of innovation programmes and standardisation activities at DIN.

Due to its many years of experience and work in cooperation with SMEs, there is an excellent network, especially for the results achieved in the project, which enables an optimal transfer of knowledge to the economy. It is intended to advance the technical development of the demonstrator to the prototype stage within the framework of a further R&D measure via the central innovation programme for SMEs of the Bundesministerium für Wirtschaft und Klimaschutz (BMWK).

7. Use of the grant

7.1 Scientific and technical staff (Subsection A.1 of the financing plan)

In detail, the work of the employees was done as follows:

- 23,7 months of scientific-technical personnel

The project management organisation has already been informed about the changes of the project processing.

7.2 Equipment (Section B of the financing plan)

As part of the project, a filament extruder was purchased as requested. The additional plastics shredding system applied for was not necessary due to the good distribution of the additives in the compounded filaments.

7.3 Services provided by third parties (Section C of the financing plan)

none

8. Necessity and appropriateness of the work done

The work carried out corresponded to the reviewed and approved application. Only the adjustment of expenditure and the transfer of these funds to staff (see Chapter 14) had to be adjusted in the course of the project. The work carried out was necessary and appropriate.

9. References

European Commission, 2012. Communication from the Commission to the European Parliament, the Council, the European Economic and Social Committee and the Committee of the Regions Report on the Review of the European Water Scarcity and Droughts Policy [online]. European Commission. https://op.europa.eu/en/publication-detail/-/publication/e5fa9abc-18da-40bd-8fe4-423d3a12f4b7/language-en/format-PDF/source-279797414

Gudkov, Burmistrov, Serov, Rebezov, Semenova and Lisitsyn, 2021. A Mini Review of Antibacterial Properties of ZnO Nanoparticles. Frontiers in Physics, 9. doi: 10.3389/fphy.2021.641481

Y. Wang, Cao, Jiang, Zhang, j. Liu, y. Liu and h. Wang, 2014. Superior Antibacterial Activity of Zinc Oxide/Graphene Oxide Composites Originating from High Zinc Concentration Localized around Bacteria. ACS Applied Materials & Interfaces, 6 (4), 2791-2798. doi: 10.1021/am4053317

Verbič, Gorjanc, and Simoničič, 2019. Zinc Oxide for Functional Textile Coatings: Recent Advances. Coatings, 9 (550). Doi: 10.3390/coatings9090550

Qi, Xing, Zada, Li, Q. Wang, Liu, Lin and G. Wang, 2020. Transition metal doped ZnO nanoparticles with enhanced photocatalytic and antibacterial performances: Experimental and DFT studies. Ceramics International, 46 (2), 1494-1502. doi: 10.1016/j.ceramint.2019.09.116

Valerini, Tammaro, Villani, Rizzo, Caputo, Paolella, and Vigliotta, 2020. Antibacterial Al-doped ZnO coatings on PLA films. Journal of Materials Science, 55, 4830-4847. doi: 10.1007/s10853-019-04311-z

Kristiawan, Imaduddin, Ariawan, U. Arifin and Z. Arifin, 2021. A review on the fused deposition modeling (FDM) 3D printing: Filament processing, materials, and printing parameters. Open Engineering 11(1). doi: 10.1515/eng-2021-0063

Y. Jung and S. Torquato, 2005. Fluid permeabilities of triply periodic minimal surfaces. Phys. Rev. E 72. doi: 10.1103/PhysRevE.72.056319

Thomas, Sreedhar, Al-Ketan, Rowshan, Al-Rub and Arafat, 2018. 3D printed triply periodic minimal surfaces as spacers for enhanced heat and mass transfer in membrane distillation. Desalination 443. doi: 10.1016/j.desal.2018.06.009

Hesselmann, Scherenberg, Bongartz, Djeljadini, Wessling, Cornelissen, Rode, Steinseifer, Jansen and Arens, 2021. Structure-dependent gas transfer performance of 3D-membranes for artificial membrane lungs. Journal of Membrane Science 634. doi: 10.1016/j.memsci.2021.119371

Feng, Fu, Yao and He, 2022. Triply periodic minimal surface (TPMS) porous structures: from multi-scale design, precise additive manufacturing to multidisciplinary applications. International Journal of Extreme Manufacturing. doi: 10.1088/2631-7990/ac5be6

10. Annex

Annex 1: Results of the particle size analysis by DLS. Every ZnO is tested three times with a newly prepared sample. PI denotes the Polydispersity Index of the given size distribution. DAF3D-2 was not available at that point in time and, given the inconclusive results, was not tested afterwards.

Test series	Mean Value (nm)	PI	10. Percentile (nm)	Median (nm)	90. Percentile (nm)
DAF3D-1 1	407	0.19	94	198	4356
DAF3D-1 2	386	0.18	102	194	421
DAF3D-1 3	490	0.22	129	184	8304
SA 1	278	0.20	212	258	315
SA 2	279	0.20	215	257	309
SA 3	278	0.19	169	272	453

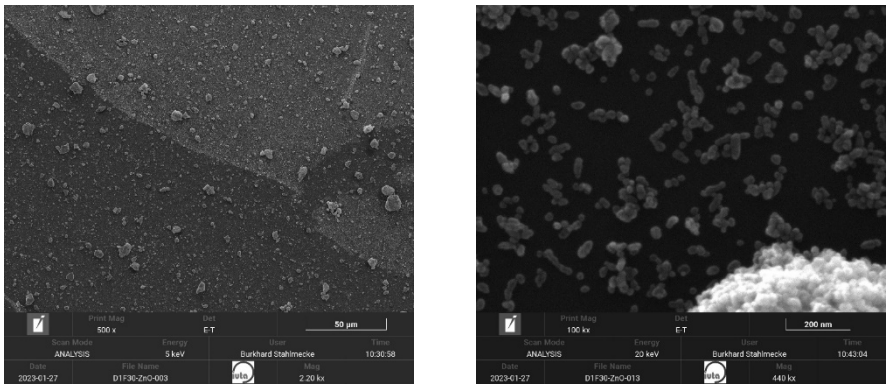

Annex 2: Exemplary images of the SEM-analysis of DAF3D-1-ZnO samples taken at a magnification of 2.2 kx (left) and 440 kx (right).

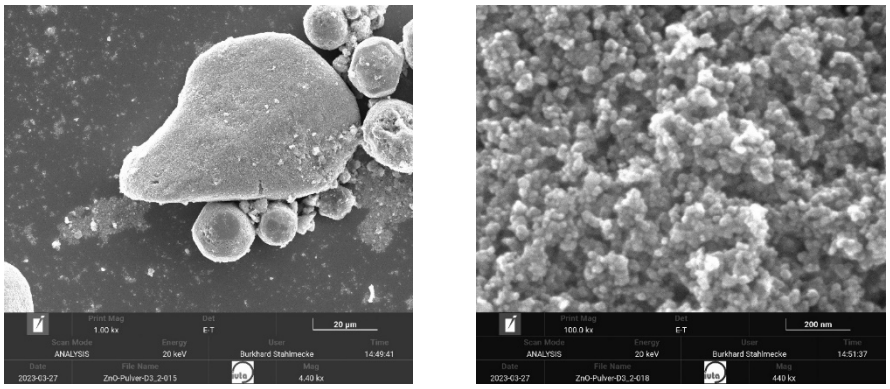

Annex 3: Exemplary images of the SEM-analysis of DAF3D-2-ZnO samples taken at a magnification of 4.4 kx (left) and 440 kx (right).

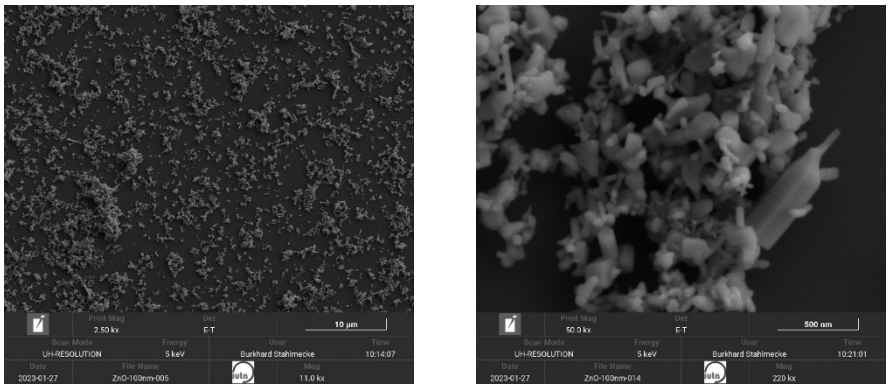

Annex 4: Exemplary images of the SEM-analysis of SA-ZnO samples taken at a magnification of 11 kx (left) and 220 kx (right).

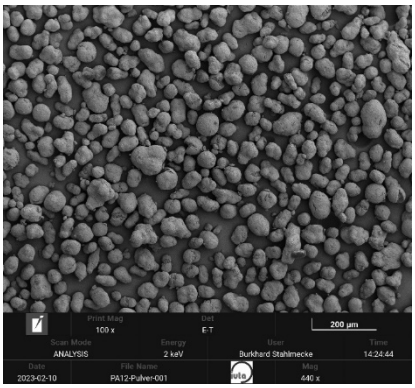

Annex 5: Exemplary image of the SEM-analysis of PA12 powder sample taken at a magnification of 440 x.

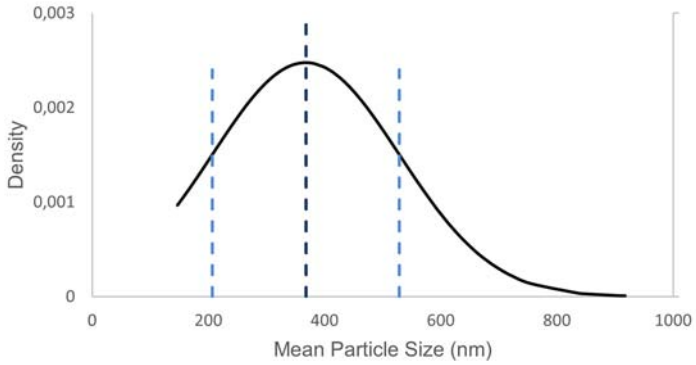

Annex 6: Mean particle size of ZnO-SA measured on the surface of 1 wt% Filament by SEM-analysis. The mean size is 367.9 nm with a standard deviation of 161 nm. Both are represented by the dotted lines.

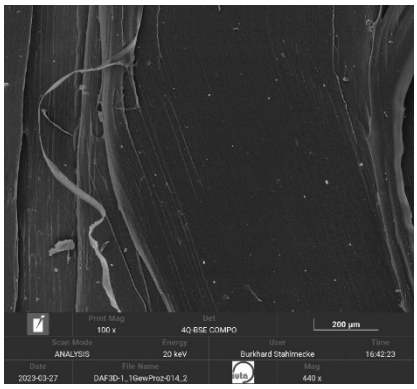
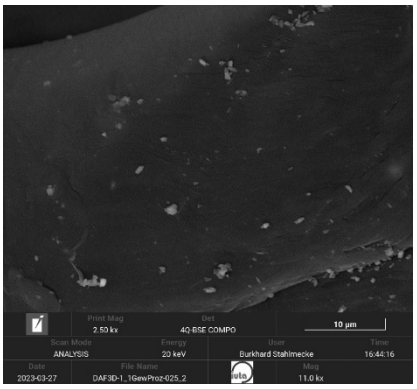

Annex 7: Exemplary images of the SEM-analysis of DAF3D-1 1 wt% printed samples taken at a magnification of 440 x (left) and 11 kx (right).

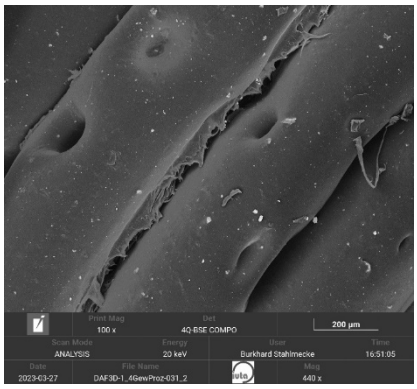
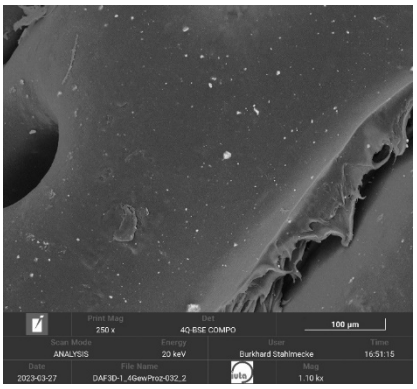

Annex 8: Exemplary images of the SEM-analysis of DAF3D-1 4 wt% printed samples taken at a magnification of 440 x (left) and 1.1 kx (right).

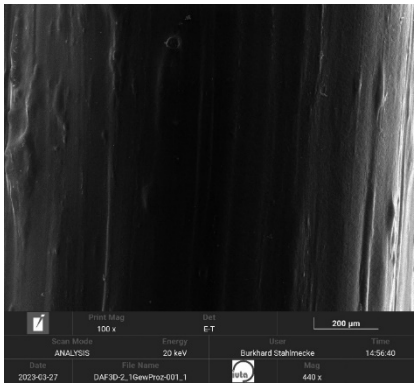
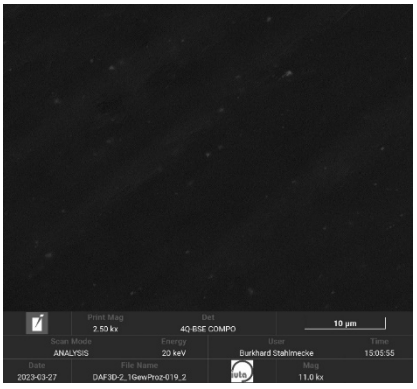

Annex 9: Exemplary images of the SEM-analysis of DAF3D-2 1 wt% filament samples taken at a magnification of 440 x (left) and 11 kx (right).

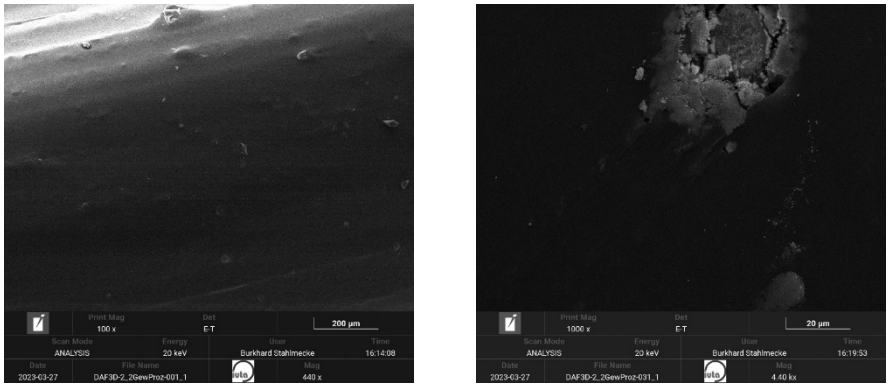

Annex 10: Exemplary images of the SEM-analysis of DAF3D-2 2 wt% filament samples taken at a magnification of 440 x (left) and 4.4 kx (right).

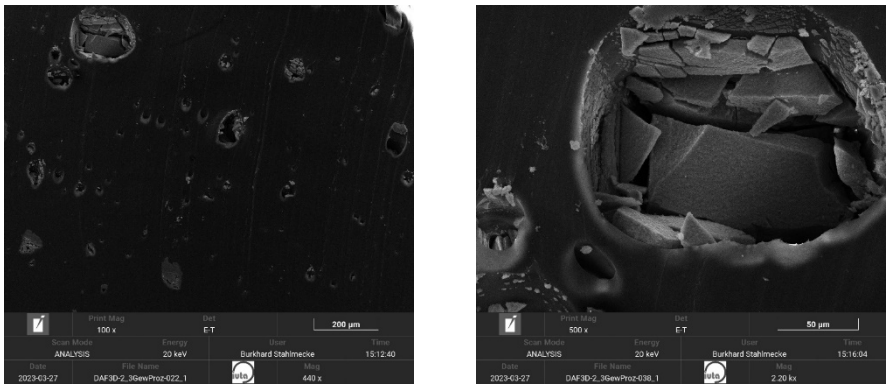

Annex 11: Exemplary images of the SEM-analysis of DAF3D-2 3 wt% filament samples taken at a magnification of 440 x (left) and 2.2 kx (right).

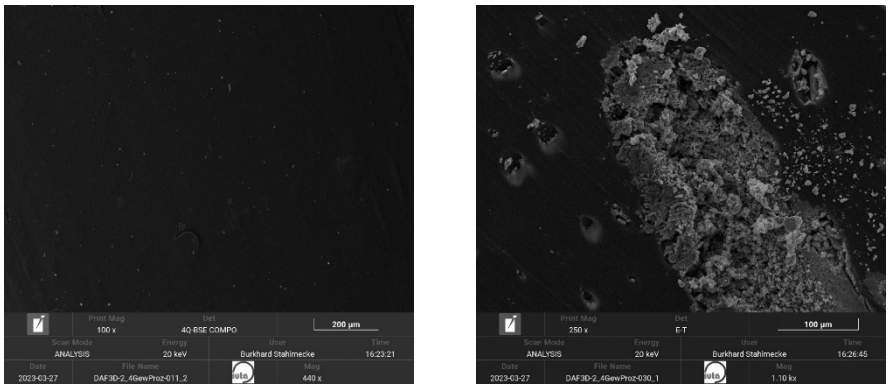

Annex 12: Exemplary images of the SEM-analysis of DAF3D-2 4 wt% filament samples taken at a magnification of 440 x (left) and 1.1 kx (right).

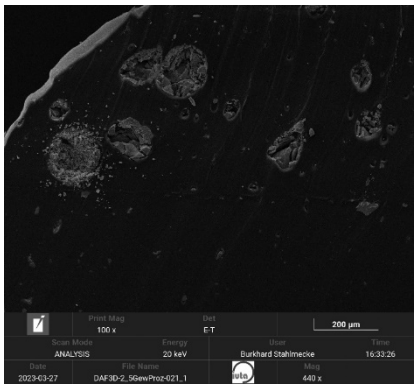

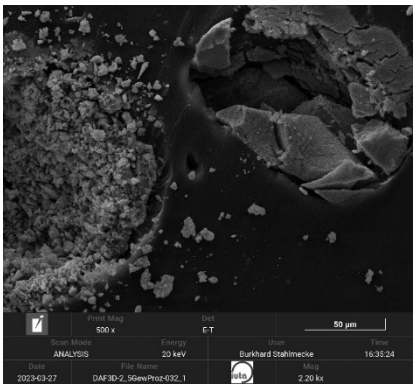

Annex 13: Exemplary images of the SEM-analysis of DAF3D-2 5 wt% filament samples taken at a magnification of 440 x (left) and 2.2 kx (right).

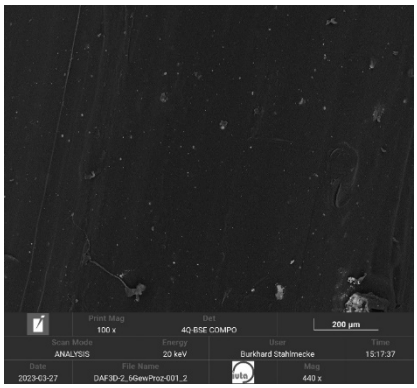

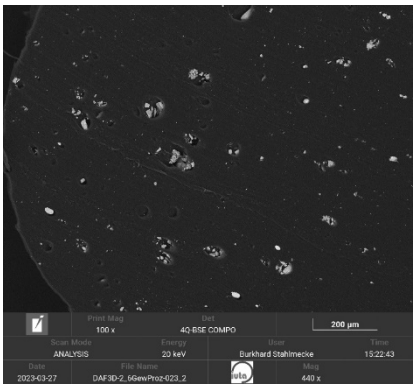

Annex 14: Exemplary images of the SEM-analysis of DAF3D-2 6 wt% filament samples taken at a magnification of 440 x at different locations of the filament surface.

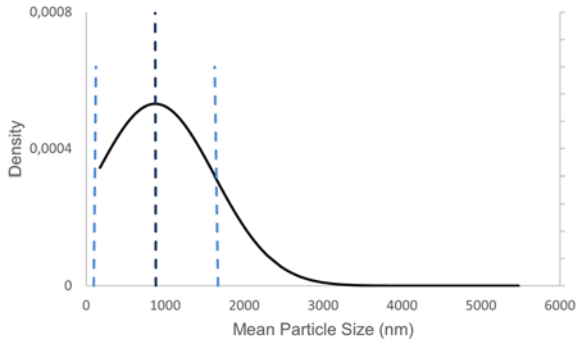

Annex 15: Mean particle size of ZnO-DAF3D-2 measured on the surface of 1 – 6 wt% filaments by SEM-analysis. The mean size is 875 nm with a standard deviation of 751 nm. Both are represented by the dotted lines. In total 692 particles were measured.

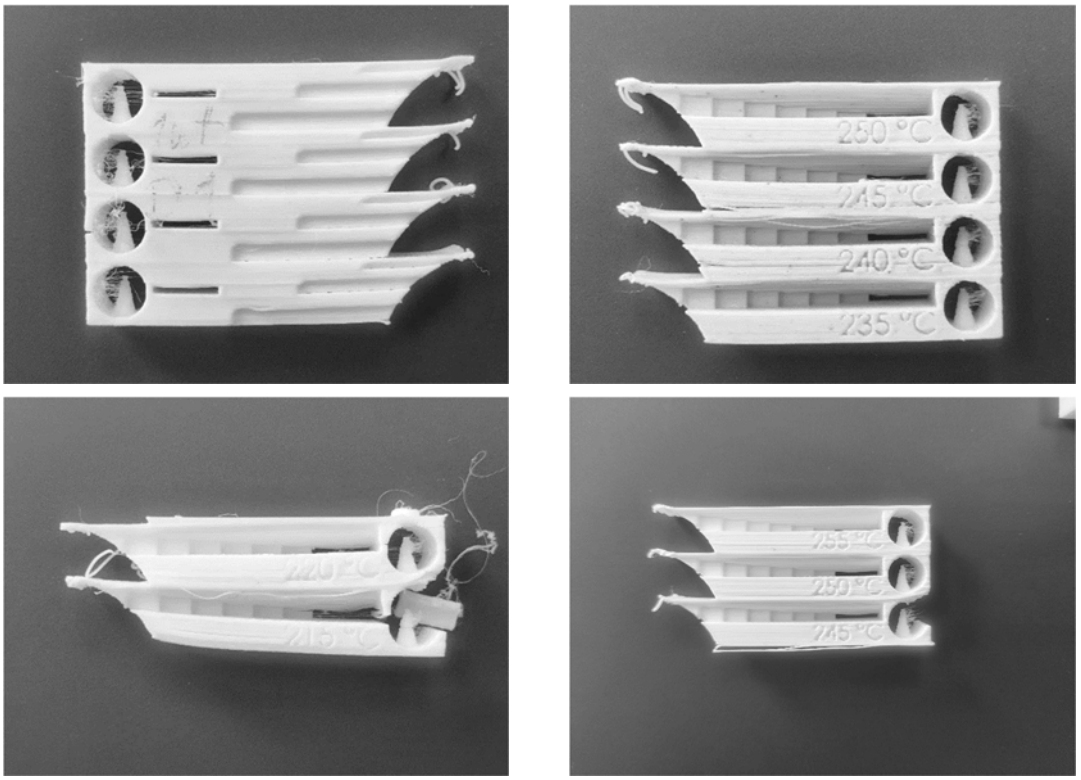

Annex 16: Temptower of different PA compounds to analyse the effect of printing temperature and other print parameters. Visible are warping, layer separations, fractures at thin structures, stringing and low hanging filament strings in bridged parts.

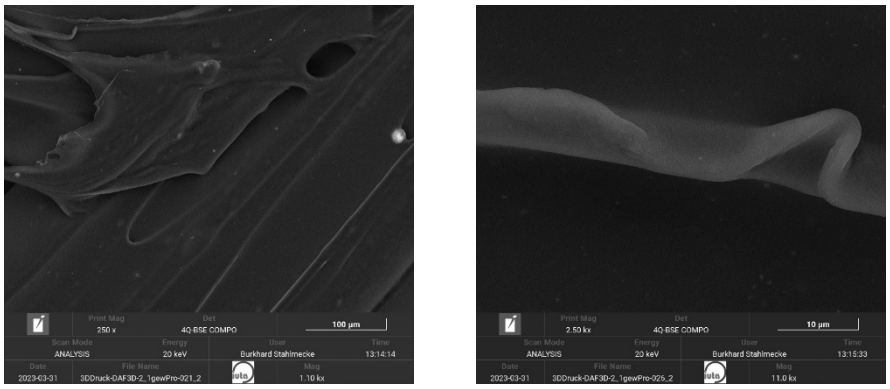

Annex 17: Exemplary images of the SEM-analysis of DAF3D-2 1 wt% printed samples taken at a magnification of 1.1 kx (left) and 11 kx (right).

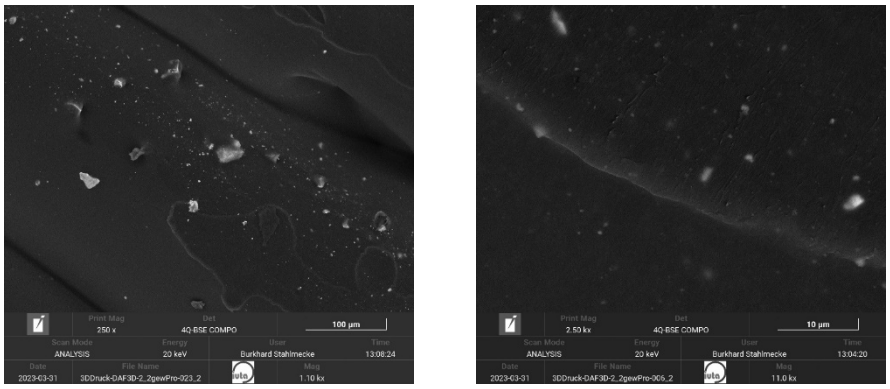

Annex 18: Exemplary images of the SEM-analysis of DAF3D-2 2 wt% printed samples taken at a magnification of 1.1 kx (left) and 11 kx (right).

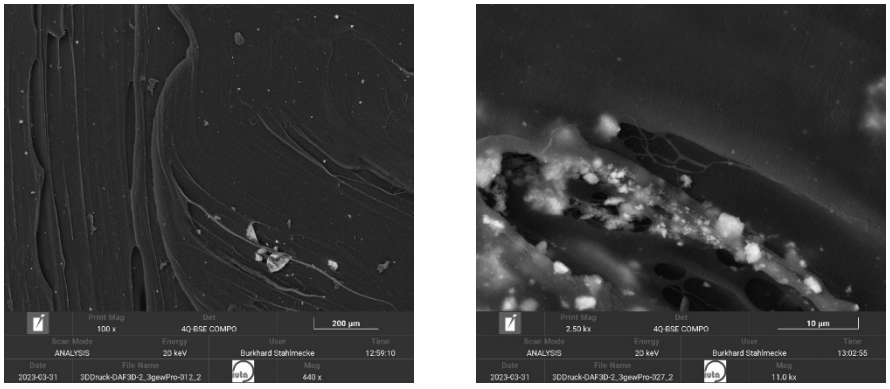

Annex 19: Exemplary images of the SEM-analysis of DAF3D-2 3 wt% printed samples taken at a magnification of 440 x (left) and 11 kx (right).

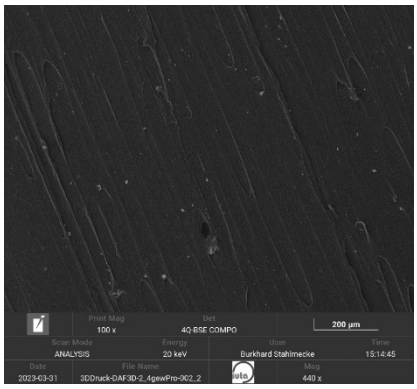
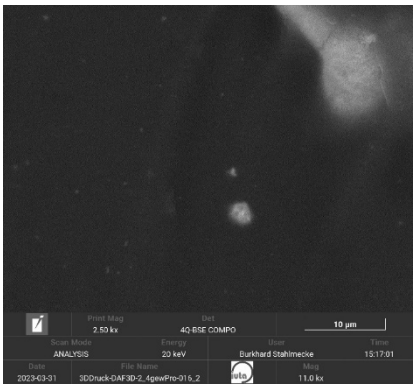

Annex 20: Exemplary images of the SEM-analysis of DAF3D-2 4 wt% printed samples taken at a magnification of 440 x (left) and 11 kx (right).

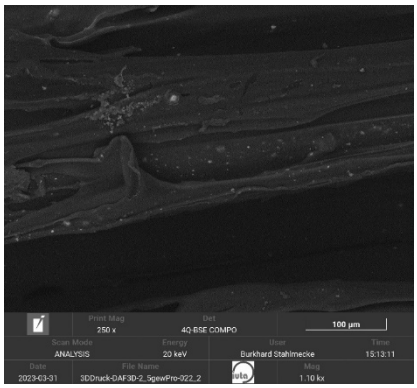
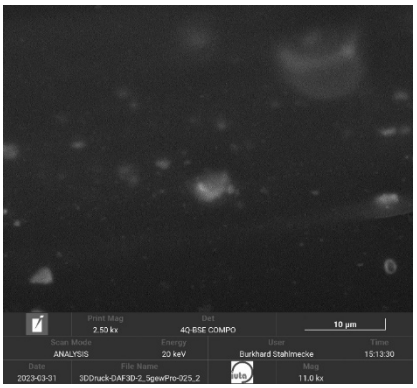

Annex 21: Exemplary images of the SEM-analysis of DAF3D-2 5 wt% printed samples taken at a magnification of 1.1 kx (left) and 11 kx (right).

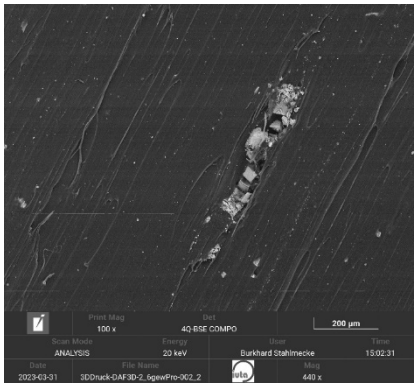
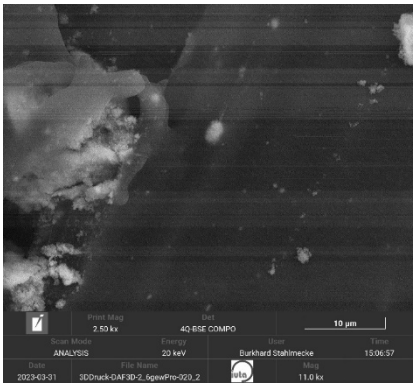

Annex 22: Exemplary images of the SEM-analysis of DAF3D-2 6 wt% printed samples taken at a magnification of 440 x (left) and 11 kx (right).

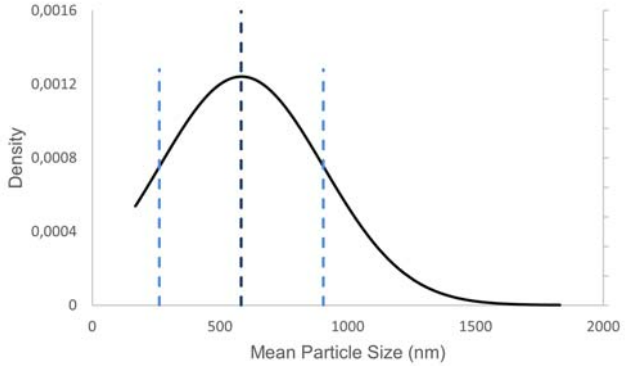

Annex 23: Mean particle size of ZnO-DAF3D-2 measured on the surface of 1 – 6 wt% printed samples by SEM-analysis. The mean size is 584 nm with a standard deviation of 321 nm. Both are represented by the dotted lines. In total 688 particles were measured.

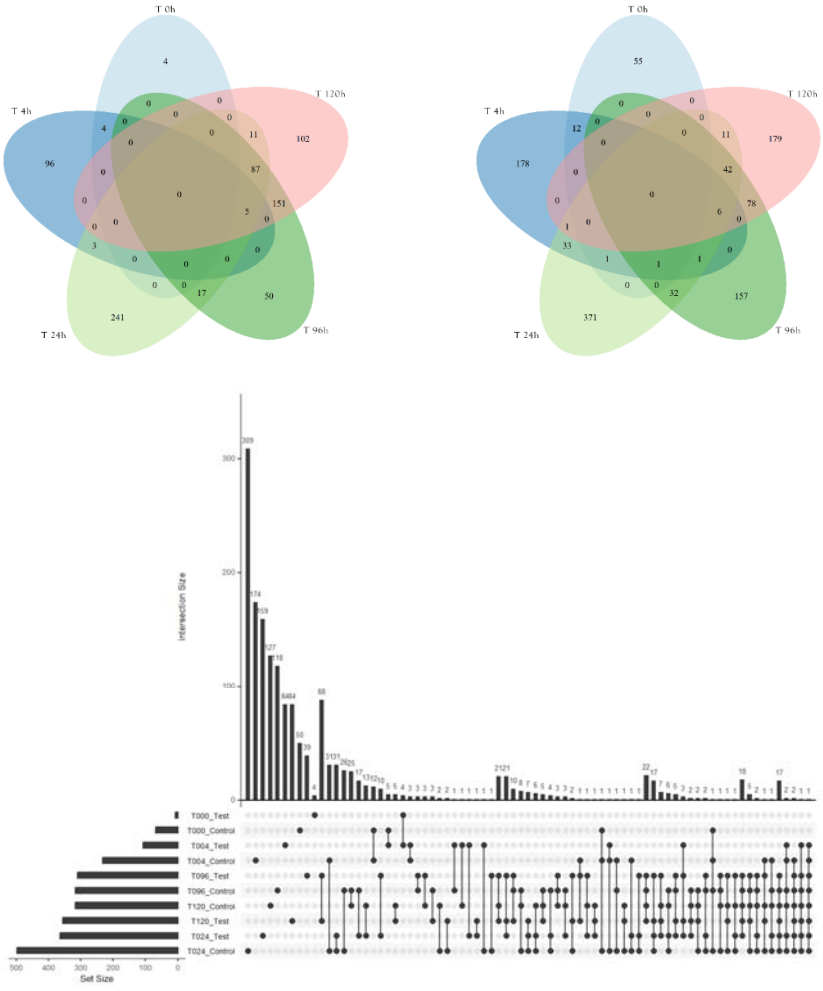

Annex 24: Venn diagrams of the NTS analysis of the ZnO-filter (left) and the corresponding control (right). Additionally, the same analysis is shown as an UpSet diagram below.